© 2022. Published by The Company of Biologists Ltd | Development (2022) 149, dev199484. doi:10.1242/dev.199484

RESEARCH ARTICLE

Regulation of retinal amacrine cell generation by miR-216b and Foxn3

Huanqing Zhang[1], Pei Zhuang[1], Ryan M. Welchko[1,*], Manhong Dai[1], Fan Meng[1,2] and David L. Turner[1,3,‡]

ABSTRACT

The mammalian retina contains a complex mixture of different types of neurons. We find that microRNA miR-216b is preferentially expressed in postmitotic retinal amacrine cells in the mouse retina, and expression of miR-216a/b and miR-217 in retina depend in part on Ptf1a, a transcription factor required for amacrine cell differentiation. Surprisingly, ectopic expression of miR-216b directed the formation of additional amacrine cells and reduced bipolar neurons in the developing retina. We identify the Foxn3 mRNA as a retinal target of miR-216b by Argonaute PAR-CLIP and reporter analysis. Inhibition of Foxn3, a transcription factor, in the postnatal developing retina by RNAi increased the formation of amacrine cells and reduced bipolar cell formation. *Foxn3* disruption by CRISPR in embryonic retinal explants also increased amacrine cell formation, whereas Foxn3 overexpression inhibited amacrine cell formation prior to Ptf1a expression. Co-expression of Foxn3 partially reversed the effects of ectopic miR-216b on retinal cell formation. Our results identify Foxn3 as a novel regulator of interneuron formation in the developing retina and suggest that miR-216b likely regulates Foxn3 and other genes in amacrine cells.

KEY WORDS: Cell fate, microRNA, Retina, Neurogenesis

INTRODUCTION

Cellular diversity is a fundamental feature of the nervous system: networks comprising different types of neurons and glia form neural circuits with distinct functional properties. The mouse retina has six major classes of neurons that can be further divided into over 100 subtypes (Clark et al., 2019; Macosko et al., 2015; Shekhar et al., 2016; Yan et al., 2020). This complex mixture of cell types performs initial visual processing. During retinal development in vertebrates, specific cell types are generated in a broadly consistent order, and individual retinal progenitor cells can give rise to combinations of differentiated cell types (reviewed by Cepko, 2014). Multiple transcriptional regulators and signaling pathways control the potential of retinal progenitor cells to generate specific cell types at different developmental times (Clark et al., 2019; Konstantinides et al., 2015; Mattar et al., 2015).

[1]Michigan Neuroscience Institute, University of Michigan, Ann Arbor, MI 48109-2200, USA. [2]Department of Psychiatry, University of Michigan, Ann Arbor, MI 48109, USA. [3]Department of Biological Chemistry, University of Michigan, Ann Arbor, MI 48109, USA.
*Present address: Neuroscience Program, College of Science and Engineering, Central Michigan University, Mt. Pleasant, MI 48859, USA.

‡Author for correspondence (dlturner@umich.edu)

P.Z., 0000-0002-8988-5735; D.L.T., 0000-0003-0080-0924

Handling Editor: Paola Arlotta
Received 31 January 2021; Accepted 7 December 2021

Amacrine cells are a diverse subset of retinal interneurons that participate in local processing of visual information (Masland, 2012). Amacrine cell subtypes can differ by neurotransmitters, morphology and other properties, with over 60 subtypes detected in the mouse by single-cell analysis of gene expression (Yan et al., 2020). During embryonic and early postnatal development, a series of transcription factors regulates the formation of amacrine cells, including the Forkhead protein Foxn4, the basic-helix-loop-helix (bHLH) proteins Ptf1a, Neurod1, Neurod4 and Ascl1, the Rorb nuclear receptor, the Meis1 homeobox, and the zinc-finger transcription factor Plagl1/Zac1 (Fujitani et al., 2006; Inoue et al., 2002; Islam et al., 2013; Li et al., 2004; Liu et al., 2013, 2020; Ma et al., 2007; Nakhai et al., 2007). Several of these factors also regulate the formation of horizontal cells, another class of interneuron, and/or other retinal neurons.

Noncoding RNAs also have been implicated as regulators of retinal development, including microRNAs (miRNAs). Mature miRNAs are ∼22 nt small RNAs that, when loaded onto Argonaute proteins, function as negative regulators of mRNA stability and translation (reviewed by Bartel, 2018). Target-miRNA interactions usually involve base-pairing between the miRNA seed sequence (positions 2-8 of the mature miRNA) and a complementary sequence in the target mRNA, often in 3′ untranslated region (3′ UTR). Loss of mature miRNAs after retina-specific disruption of the miRNA processing enzyme Dicer leads to altered production of retinal cell types, including fewer amacrine cells, with prolonged generation of early cell types (Davis et al., 2011; Georgi and Reh, 2010) and/or widespread cell death (Damiani et al., 2008), depending on the timing of Dicer disruption. miRNAs have been implicated in the differentiation or maintenance of retinal neurons and Müller glia, as well as in the neurogenic potential of Müller glia (Kara et al., 2019; Reh and Hindges, 2018; Walker and Harland, 2009; Wohl et al., 2017, 2019; Xiang et al., 2017).

Here, we show that ectopic expression of the miR-216b miRNA during mouse retinal development leads to an increase in amacrine cells and a decrease in bipolar cells. miR-216b is normally expressed in differentiated amacrine cells, starting during retinal development. We identify the 3′ UTR of the mRNA encoding the Foxn3 transcription factor as a target of miR-216b. Inhibition of Foxn3 by RNAi or CRISPR disruption in developing retinas leads to an increase in amacrine cells, whereas overexpression of Foxn3 reduces amacrine cell number and co-expression of Foxn3 with miR-216b can partially reverse the effects of miR-216b. Our observations identify Foxn3 as a novel regulator of retinal interneuron formation and suggest that miR-216b is a regulator of gene expression in amacrine cells.

RESULTS

To identify miRNAs enriched in retinal amacrine cells, we used small RNA sequencing to compare miRNA levels in embryonic day 18.5 (E18.5) retinas isolated from mice heterozygous or

Development (2022) 149, dev199484. doi:10.1242/dev.199484

homozygous for disruption of the gene encoding Ptf1a, a transcription factor required for formation of most amacrine and horizontal cells in the retina (Fujitani et al., 2006; Nakhai et al., 2007). In retinas without *Ptf1a*, several miRNAs were reduced relative to the retinas from *Ptf1a* heterozygotes, with miR-216b-5p the most downregulated miRNA (Fig. 1A, Table S1). *Mir216b* is part of a genomic miRNA cluster with *Mir216a* and *Mir217*; miR-216a-5p/3p and miR-217-5p also were decreased in Ptf1a knockout retinas. Real-time quantitative reverse-transcription PCR (qRT-PCR) confirmed downregulation of the predominant mature miRNAs from these miRNA genes in E18.5 Ptf1a knockout retinas, relative to retinas from heterozygotes (Fig. 1B). A developmental time course of retinal expression by qRT-PCR showed that all three mature miRNAs decreased from postnatal day 0 (P0) to P7 but were still expressed in P12 and adult retinas. In contrast, miR-183-5p, an unrelated miRNA expressed in photoreceptors and bipolar cells (Xu et al., 2007; Zhuang et al., 2020), increased between P0 and adult (Fig. 1C). miRNA *in situ* hybridization for mature miR-216b-5p revealed expression in the inner retina at P0 and in the inner nuclear layer (INL) and in the ganglion cell layer (GCL) at P12, with the strongest signal at P12 in the amacrine layers of the inner INL (Fig. 1D). Expression was substantially lower or absent in the neuroblast layer at P0 and the ONL at P12. Cells labeled by miR-216b-5p *in situ* hybridization overlapped with the amacrine cell-specific transcription factor AP2α (Tfap2a) (Bassett et al., 2007) at P0 or P12 (Fig. 1E-J). miR-216b-5p also overlaps with AP2α at E18.5 in retinas, but miR-216b-5p was reduced and AP2α was absent in Ptf1a knockout retinas (Fig. S1). *In situ* hybridization for miR-216b-5p, miR-216a-5p and miR-217-5p in retinas at different ages revealed expression in INL and GCL (Fig. 1D and Fig. S2). At P0, expression was detected in inner retina, but the miRNAs were present at low levels or not expressed in the neuroblast layer. Reduced expression in Ptf1a mutant retinas and localization to the inner retina are consistent with expression of all three miRNAs in postmitotic amacrine cells.

The miR-216a/b miRNAs can promote amacrine cell formation

The miR-216a-5p and miR-216b-5p miRNAs have similar seed sequences and potentially could bind to overlapping sets of target sites, whereas miR-217-5p has a distinct seed sequence and is expected to bind to different target sites (Fig. 2A). To determine whether miR-216a/miR-216b/miR-217 could influence retinal development, we ectopically expressed these miRNAs in neonatal mouse retinas. DNA plasmid vectors that express GFP with pre-miR-216b, pre-miR-216a or pre-miR-217 expressed from the intron of the same transcription unit (Fig. 2A), either together or individually, were introduced into P0 mouse retinas by *in vivo* electroporation (Matsuda and Cepko, 2004; Zhang et al., 2012). GFP expression was used to identify electroporated cells. Ectopic

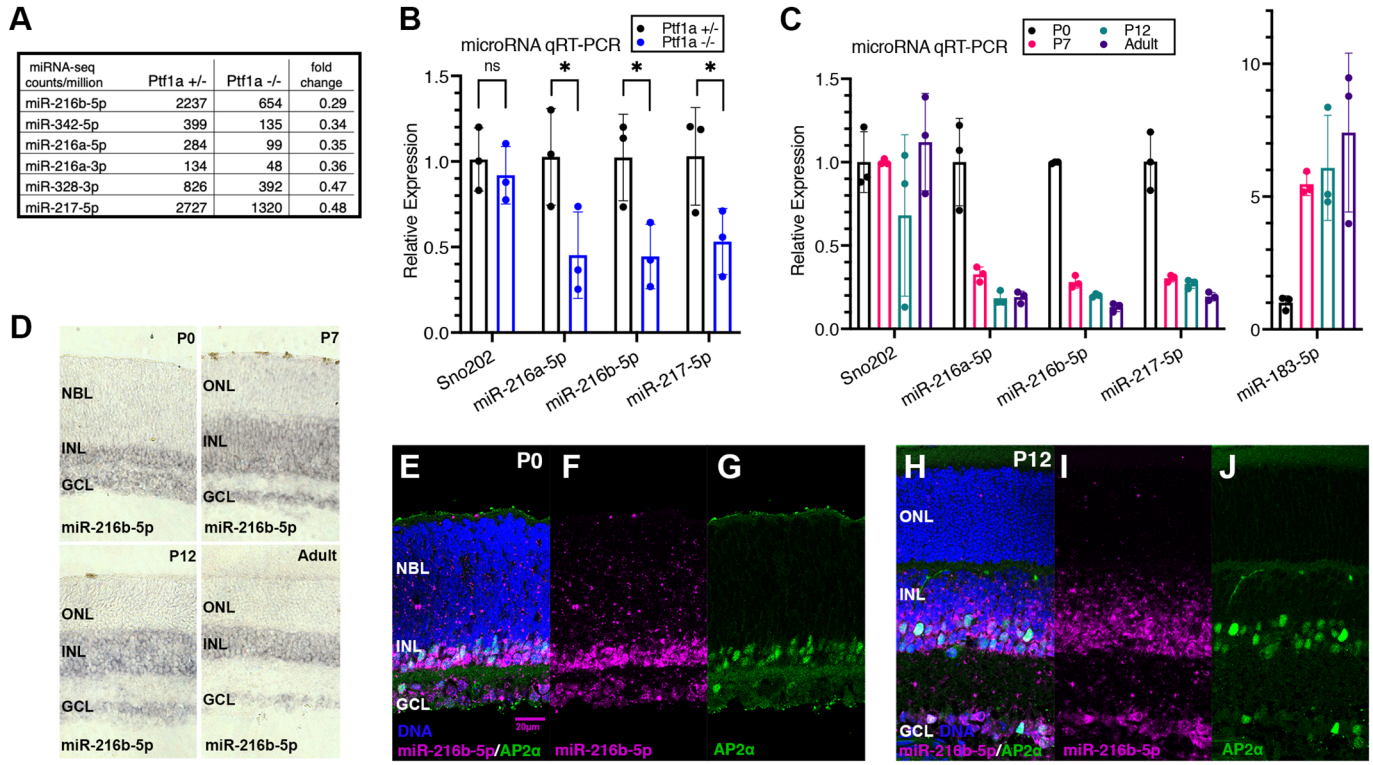

Fig. 1. Expression of miR-216a/b and miR-217 miRNAs in mouse retina. (A) miRNAs with the largest fold decrease in small RNA-sequencing counts (mean, n=2) in retinas from E18.5 Ptf1a homozygous null mice, relative to retinas from Ptf1a heterozygous mice (among miRNAs with minimum 100 counts per million mean reads in Ptf1a heterozygous samples). (B) qRT-PCR for mature miR-216a-5p, miR-216b-5p and miR-217-5p shows reduced expression in E18.5 Ptf1a homozygous retinas, while Sno202 control is unchanged (n=3). Significance is based on a one-tailed, unpaired t-test: *P<0.05. Data are mean±s.d. with individual data points indicated. (C) Mature miR-216a-5p, miR-216b-5p and miR-217-5p expression decreases in wild-type retinas after P0, but expression persists in adult retinas. In contrast, the rod and bipolar miRNA miR-183-5p increases after P0 in the same samples (n=3). (D) miR-216b-5p expression, detected by miRNA *in situ* hybridization (purple), overlaps with differentiated retinal cells in inner retina at P0 and high level expression is restricted to the INL and GCL in P7, P12 and adult retinas, with the strongest signal in the amacrine cell layer. (E-J) miR-216b-5p expression detected by miRNA fluorescent *in situ* hybridization (magenta), overlaps with amacrine cell-specific AP2α protein detected by immunofluorescence (green) at P0 (E-G) and P12 (H-J). NBL, neuroblast layer; INL, inner nuclear layer; GCL, ganglion cell layer; ONL, outer nuclear layer.

Development (2022) 149, dev199484. doi:10.1242/dev.199484

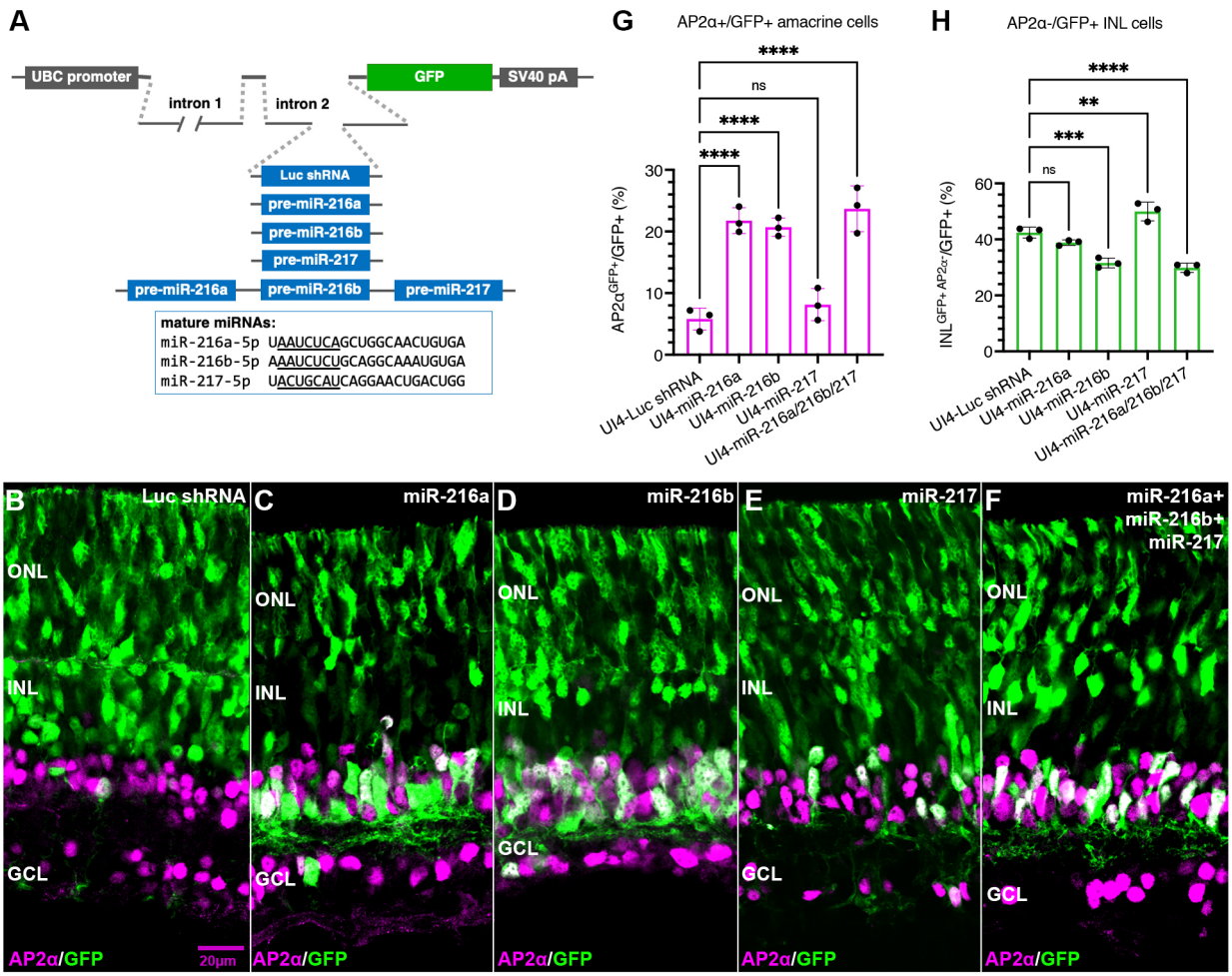

Fig. 2. miR-216a/b can promote amacrine cell formation in the developing mouse retina. (A) Schematic of plasmid miRNA expression vectors, which co-express GFP with one or three pre-miRNA(s), or a control Luc shRNA based on pre-miR-155, from an intron in the GFP mRNA. Mature miRNA sequences are shown, with seed sequences underlined. Plasmid vectors were introduced into the retina by *in vivo* electroporation at P0; retinas were analyzed at P7. (B) Widespread GFP-labeled cells were observed in ONL and outer INL after introduction of the control vector, with some GFP-labeled, AP2α-expressing amacrine cells. (C-E) Expression of miR-216a (C) or miR-216b (D), but not miR-217 (E), led to increased AP2α$^+$ amacrine cells among GFP-labeled cells, and loss of GFP-labeled cells in the outer part of the INL. (F) Co-expression of all three miRNAs was similar to expression of miR-216a or miR-216b individually. Quantitation is shown in G,H. Data are mean±s.d. with individual data points indicated. n=3; significance is based on one-way ANOVA with Dunnett's multiple comparisons test: **P<0.01, ***P<0.001, ****P<0.0001; ns, not significant. INL, inner nuclear layer; GCL, ganglion cell layer; ONL, outer nuclear layer.

miR-216b expression was confirmed by *in situ* hybridization (Fig. S3). A plasmid vector expressing GFP and a pre-miR-155-based shRNA against luciferase was used as a control [a functional synthetic miRNA with no detectable effect on the retina (Zhang et al., 2012)]. Forced expression of miR-216a, miR-216b or all three miRNAs together led to a significant increase in the frequency of amacrine cells among GFP-labeled cells at P7, relative to control, as assessed by immunodetection of AP2α (Fig. 2B-G). Introduction of miR-216b or miR-216a individually yielded similar increases in amacrine cells among the GFP-labeled cells, whereas introduction of miR-217 by itself did not (Fig. 2E,G). Although control retinas had few or no GFP-labeled displaced amacrine cells in the GCL, we observed occasional GFP-labeled amacrine cells in the GCL after electroporation with miR-216b, miR-216a or miR-216a/miR-216b/miR-217 together. In addition, AP2α-negative GFP-labeled cells in the INL decreased after expression of miR-216b or all three miRNAs together (Fig. 2D,F,H), suggesting a decrease in bipolar neurons among the electroporated cells. Although antibody markers specific for bipolar cells did not work well at P7, additional experiments described below show that miR-216b decreases bipolar cell frequency among the electroporated cells when scored at P12.

Homozygous disruption of *Ptf1a* leads to nearly complete loss of amacrine cells (Fujitani et al., 2006). As miR-216a/b expression depends in part on Ptf1a, we investigated whether expression of miR-216b would be sufficient to direct formation of amacrine cells in retinas without Ptf1a. Expression vectors for miR-216b or the Luc shRNA control were introduced by electroporation into E16.5 retinas from mice heterozygous or homozygous for disruption of *Ptf1a*. As *Ptf1a* knockout mice are not viable after birth, retinas were maintained as explants *in vitro* and assessed for AP2α expression at 8 days *in vitro* (DIV). The miR-216b expression vector failed to generate AP2α-labeled cells in the absence of Ptf1a (Fig. S4), indicating that miR-216b cannot direct formation of amacrine cells without Ptf1a.

Foxn3 is a target of miR-216b in the retina

We used Argonaute PAR-CLIP (Hafner et al., 2010) to identify potential endogenous miRNA targets in developing retina, including targets of miR-216a/b. P0 mouse retinas were cultured

Development (2022) 149, dev199484. doi:10.1242/dev.199484

as explants in 4-thiouridine (4SU) containing media for one DIV. After UV crosslinking and lysis, endogenous Argonaute 1-4 proteins with crosslinked RNA were immunoprecipitated and cDNA libraries were prepared from the RNA fragments using a modified PAR-CLIP method, then analyzed by high-throughput sequencing (see Materials and Methods). We generated five independent libraries from Argonaute immunoprecipitations and two control libraries from IgG immunoprecipitations. PAR-CLIP with 4SU frequently generates T to C substitutions at crosslinks during reverse transcription, allowing single base resolution of crosslink positions (Hafner et al., 2010). To distinguish crosslinks from random sequencing errors, we identified mapped sequences with consistent T to C substitutions at the same genomic position in two or more Argonaute PAR-CLIP libraries, without a T to C substitution at the same position in control libraries. For multiple closely spaced crosslinks, we identified the most frequent crosslink (±15 nt around each crosslink) to create a set of 14,054 most frequent, consistent crosslink sites, which we refer to as predominant crosslinks. Most predominant crosslink sites were in 3′ untranslated regions (UTRs) of mRNAs, with coding regions the next most frequent location (Fig. 3A), similar to prior PAR-CLIP analyses of Argonaute (Hafner et al., 2010; Lipchina et al., 2011). As lysates included both cytoplasm and nuclei, nuclear Argonaute likely contributed to crosslinked sites in introns and ncRNAs (Sarshad et al., 2018).

Argonaute PAR-CLIP frequently generates crosslinks in target RNAs within a few nucleotides of a bound miRNA seed sequence (Hafner et al., 2010). We looked at the distribution of sequences complementary to miRNA seed sequences within ±15 nt windows centered on a subset of predominant crosslink sites that mapped to 3′ UTRs. Seed matches for 15 miRNA seeds present in retinas at P0 were strongly enriched near crosslink sites (Fig. S5). Based on these results, and additional results described below, we conclude that Argonaute PAR-CLIP identified retinal miRNA-binding sites. Here, we analyze potential miR-216a/b sites in the Argonaute PAR-CLIP data; analysis of other retinal miRNA binding sites will be described elsewhere.

Seed matches were identified for miR-216a/b-5p near 404 predominant crosslink positions (Tables S3 and S4). miR-216a-5p and miR-216b-5p differ at position 8 (last base of the seed, Fig. 2A). As both miRNAs function similarly when expressed in retinas, we focused on sites with a match to positions 2-7 of both miRNAs, without a match to a more abundant miRNA seed or a seed match located closer to the crosslink site. We identified 57 predominant crosslink sites that met these criteria (Table S3). The site with the largest number of crosslinks near a miR-216a/b-5p 2-7 seed match was in the 3′ UTR of the Foxn3 transcription factor mRNA; crosslinks at this site were present in all five Argonaute PAR-CLIP libraries (Fig. 3B,C). We also assessed evolutionary conservation of predicted seed sites and the miR-216a/b-5p seed match in the Foxn3 3′ UTR is conserved to chickens and fish (Fig. 3D, Table S3).

We constructed a Luciferase reporter with the first 266 nt of 3′ UTR from Foxn3 (Fig. 4A). The Foxn3 3′ UTR fragment included both the frequently crosslinked miR-216a/b-5p site, as well as a second potential miR-216a/b-5p site near the stop codon. The second site had T to C substitutions in two distinct reads in one retinal PAR-CLIP library and therefore was not identified as a consistent crosslink site. In HEK293 cells in culture, the Foxn3 3′

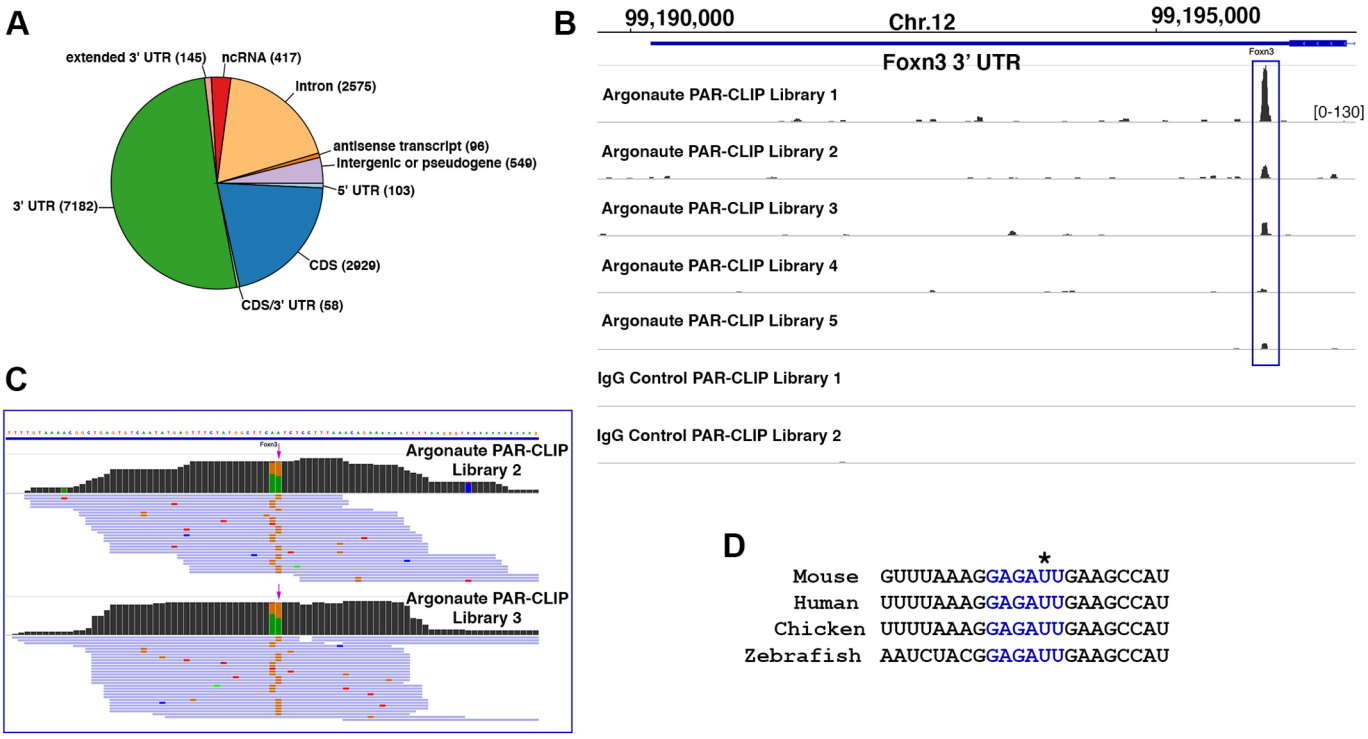

Fig. 3. Argonaute PAR-CLIP identifies Foxn3 as a miR-216a/b target. (A) 14,054 predominant Argonaute PAR-CLIP crosslink sites in neonatal retinas were mapped to genomic annotations. Most sites were in 3′ UTRs: but sites were present in other features (extended 3′ UTR: <1 kb 3′ to an annotated 3′ UTR). (B) A peak of overlapping PAR-CLIP read coverage (blue box) was present in the Foxn3 3′ UTR, with crosslinked reads present in all five Argonaute libraries, but not in two IgG control libraries. Same vertical scale for all libraries. (C) Genomic reads mapped to Foxn3 3′ UTR, showing the peak region from Argonaute libraries 2 and 3. Foxn3 is transcribed from the minus strand, so crosslinks appear as A to G substitutions (orange) on the genomic plus strand. The predominant crosslink sites are indicated by arrows. (D) miR-216a/b seed match (blue) near the predominant crosslink site in mouse Foxn3 3′ UTR (indicated by an asterisk) is evolutionarily conserved in other vertebrates.

Development (2022) 149, dev199484. doi:10.1242/dev.199484

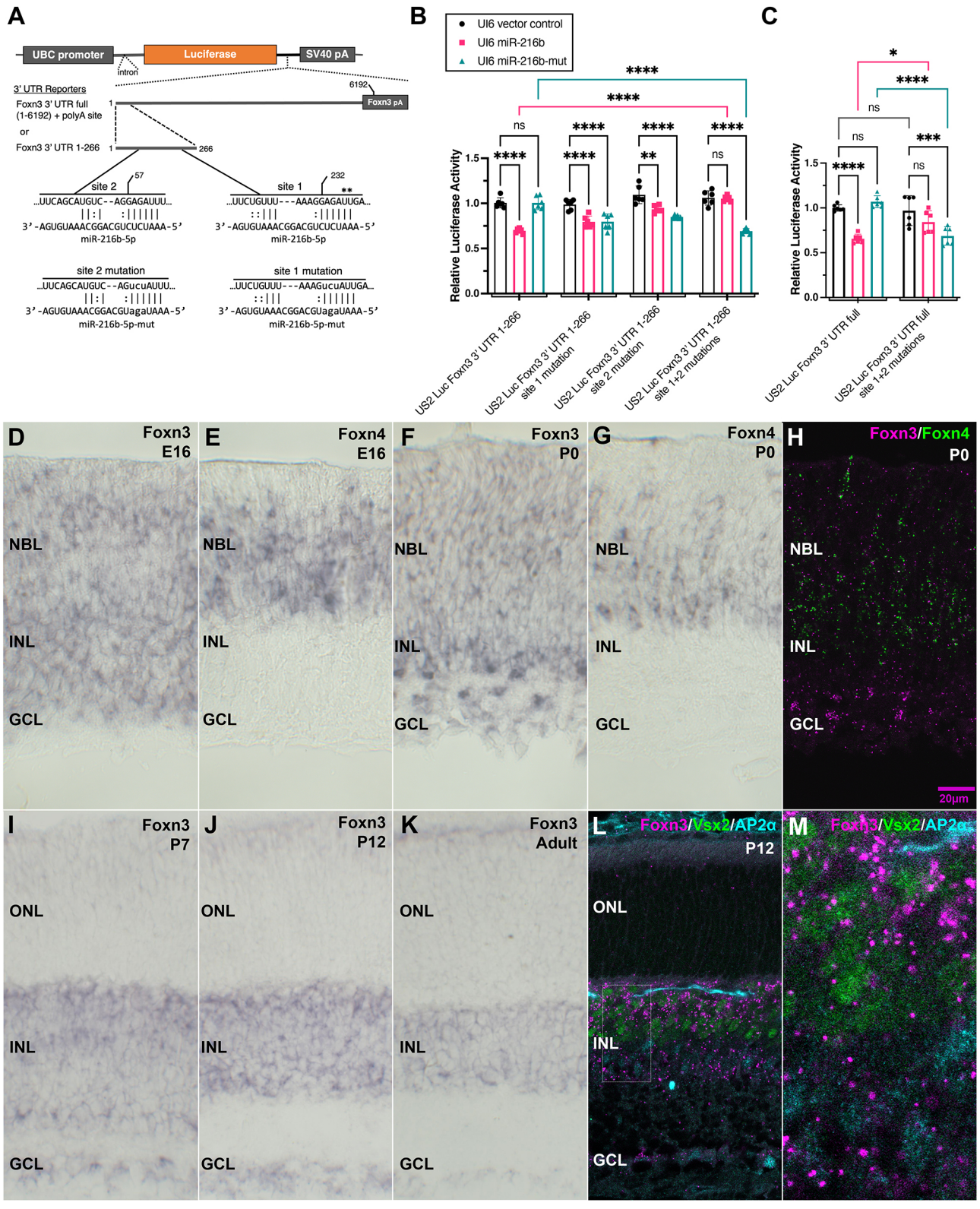

Fig. 4. See next page for legend.

UTR 1-266 reporter was inhibited by co-transfection of the miR-216b expression vector but not the miR-216b-mut expression vector, which expresses a version of pre-miR-216b with a seed sequence mutation in miR-216b-5p (and compensating changes in the 3′ end of miR-216b-3p to allow folding of the precursor). A reporter in which both seed matches in the Foxn3 3′ UTR fragment were mutated was not inhibited by the miR-216b vector. However, the miR-216b-mut vector downregulated the reporters with mutated miR-216a/b-5p sites, as we used compensatory site mutations in the Foxn3 3′ UTR fragment, complementary to the seed sequence in

Development (2022) 149, dev199484. doi:10.1242/dev.199484

Fig. 4. Repression of the 3′ UTR of Foxn3 by miR-216b; Foxn3 mRNA expression during retinal development overlaps with Foxn4 expression. (A) Schematic of two luciferase reporters: positions 1-266 of the Foxn3 3′ UTR, which contains two miR-216a-5p/b-5p seed matches (most frequent Argonaute PAR-CLIP crosslinking sites near site 1 indicated by asterisks), and a reporter based on full-length Foxn3 3′ UTR. The miR-216b-mut miRNA with an altered seed sequence is shown, as well as Foxn3 3′ UTR site mutations that it can pair with (lower case letters indicate substituted bases). (B) The Foxn3 3′ UTR 1-266 luciferase reporter is repressed by co-expression of miR-216b in HEK293 cells, but not by co-expression of miR-216b-mut. Mutation of both seed matches in the reporter to match the seed in miR-216b-mut prevents repression by miR-216b and allows repression by miR-216b-mut, while single seed match mutations allow repression by either miRNA. (C) The full-length 3′ UTR reporter is repressed by co-expression of miR-216b, but not by co-expression of miR-216b-mut. Mutation of the two miR-216b sites reduces repression by miR-216b and allows repression by miR-216b-mut. (B,C) n=6; significance for selected comparisons indicated, based on two-way ANOVA with Tukey's multiple comparisons test: *P<0.05, **P<0.01, ***P<0.001, ****P<0.0001; ns, not significant. Data are mean±s.d. with individual data points indicated. (D-G,I-K) Expression of Foxn3 or Foxn4 mRNAs (purple) in the developing retina at indicated ages, detected by *in situ* hybridization. Foxn3 is expressed in the neuroblast layer and in a subset of differentiated cells in INL/GCL, whereas Foxn4 is restricted to a subset of neuroblast layer cells. (H) Overlap between Foxn3 (magenta) and Foxn4 (green) expression in cells of the P0 retina, detected by *in situ* hybridization chain reaction (HCR). (L) Foxn3 mRNA in the INL at P12 (magenta), detected by *in situ* HCR, overlaps with Vsx2, a marker for bipolar cells (green) and a small number of amacrine cells (AP2α, cyan), detected by immunofluorescence. (M) Enlargement of the boxed region in L. NBL, neuroblast layer; INL, inner nuclear layer; GCL, ganglion cell layer; ONL, outer nuclear layer.

miR-216b-5p-mut (Fig. 4A,B). We also constructed a Luciferase reporter with the full-length Foxn3 3′ UTR (6192 nt) and polyadenylation site (Fig. 4A,C). The full-length Foxn3 3′ UTR reporter was inhibited by co-transfection of the miR-216b expression vector, but not the miR-216b-mut expression vector, in HEK293 cells. Mutation of the two miR-216a/b-5p sites in the full length 3′ UTR prevented significant repression by miR-216b, but allowed the full UTR reporter to be repressed by the matching miR-216b-mut. These observations indicate that the Foxn3 3′ UTR is a miR-216b-5p target.

Intriguingly, Foxn3 is closely related to Foxn4, a transcription factor required for the initial steps of amacrine cell formation (Li et al., 2004). However, although Foxn4 is a transcriptional activator (Lelièvre et al., 2012; Liu et al., 2013), Foxn3 is a transcriptional repressor (Scott and Plon, 2005). This difference suggested that Foxn3 might inhibit amacrine cell formation, so that miR-216a/b inhibition of Foxn3 could allow increased amacrine cell formation. Foxn3 is expressed in the head and eye in vertebrates, and reduced Foxn3 function leads to a small eye phenotype in *Xenopus* and mice, as well as head neural crest defects (Samaan et al., 2010; Schuff et al., 2007). However, a role for Foxn3 in the generation of specific retinal cell types has not been described. We therefore further analyzed expression of Foxn3 during mouse retinal development. At E16.5 or P0, we detected widespread expression of Foxn3 mRNA in mouse retina by *in situ* hybridization, both in the neuroblast layer and in some differentiating cells of the inner retina (Fig. 4D,F). We compared Foxn3 expression with Foxn4, which is expressed in retinal precursor cells that can generate amacrine interneurons. Foxn4 mRNA was restricted to cells in the neuroblast layer at E16.5 or P0, consistent with previous reports (Li et al., 2004), and a subset of cells expressed both Foxn3 and Foxn4 mRNAs at P0 or E16.5 (Fig. 4D-H, Fig. S6). In P7, P12 and adult retinas, Foxn3 expression was restricted to INL and GCL, with most expressing cells in the outer INL (Fig. 4I-K) at P7 and P12. Foxn3 mRNA expression in INL overlaps with markers of bipolar cells and a small subset of amacrine cells at P12 (Fig. 4L,M; Fig. S7). Based on recent single cell sequencing data for amacrine cells (Yan et al., 2020), Foxn3 mRNA expression was correlated with genes expressed in cholinergic amacrine cells, such as Sox2, and the highest level of Foxn3 mRNA was present in cholinergic amacrine cells (Table S5).

Foxn3 modulates amacrine cell and bipolar cell formation

To determine whether reduced Foxn3 expression affects amacrine cell formation, we inhibited Foxn3 with shRNAs in developing retinas. We used RNA polymerase II-driven shRNA vectors that co-express GFP and miR-155-based shRNAs (Chung et al., 2006). Because an antibody suitable for immunodetection of mouse Foxn3 is not available, we confirmed the ability of each shRNA to reduce endogenous Foxn3 mRNA in a mouse cell line using qRT-PCR (Fig. S8), although the shRNA 635 reduced Foxn3 mRNA more effectively. The shRNA vectors were delivered into P0 retinas by *in vivo* electroporation. In parallel, we electroporated the control Luc shRNA vector, the expression vector for miR-216b or the miR-216b-mut expression vector. We observed a significantly increased proportion of AP2α-positive amacrine cells among the GFP-labeled cells in retinas collected at P12 with Foxn3 shRNA 635, the more effective shRNA, relative to the control shRNA vector, whereas a smaller increase with Foxn3 shRNA 195 was not significant (Fig. 5A-C,K). miR-216b expression also increased the fraction of amacrine cells among the GFP-labeled cells at P12, whereas miR-216b-mut expression did not (Fig. 5D,E,K). The fraction of Vsx2 (also known as Chx10) -positive bipolar cells among the GFP-labeled cells decreased with Foxn3 shRNA 195, Foxn3 shRNA 635 and miR-216b (Fig. 5F-I,L). Expression of miR-216b-mut did not significantly decrease the fraction of bipolar cells among GFP-labeled cells (Fig. 5J,L). These results indicate that the miR-216b vector likely alters retinal development via target repression through the miR-216b-5p strand/seed, and that inhibition of Foxn3 in the developing retina yields changes in retinal cell types similar to changes seen after overexpression of miR-216b.

As an independent test of Foxn3 function, we used CRISPR/Cas9 (Sarin et al., 2018; Wang et al., 2014) to disrupt the Foxn3 gene in embryonic retina explants in culture, then assessed changes in amacrine cell number. Two different Cas9/sgRNA expression vectors, each expressing GFP and two independent sgRNAs against Foxn3, or a control Cas9/GFP vector were electroporated into mouse retinas at E16.5, prior to the peak of amacrine cell generation, and the retinas were maintained as explants for 8 DIV. We observed an increased fraction of AP2α$^+$ cells among the GFP-labeled cells in explants with either of the CRISPR vectors targeting Foxn3, relative to the control vector (Fig. 6A-F). To confirm Cas9 disruption of the Foxn3 gene in retinal cells after electroporation with CRISPR vectors at E16.5, we amplified the four genomic targets by PCR from GFP-positive retina explants at 2 DIV, then detected indels by Illumina sequencing of the PCR products. For each vector targeting Foxn3, one of the two sgRNAs was effective (Fig. S9, Table S6). The increase in amacrine cell fraction after CRISPR disruption of Foxn3 is similar to the results observed after postnatal inhibition of Foxn3 by RNAi. These results indicate that reduced Foxn3 function in cells of the developing retina permits increased amacrine cell formation.

To assess the consequences of Foxn3 overexpression in developing retinas, we introduced expression vectors for a Foxn3 cDNA (without its 3′ UTR) and GFP into E16.5 retinas by

Development (2022) 149, dev199484. doi:10.1242/dev.199484

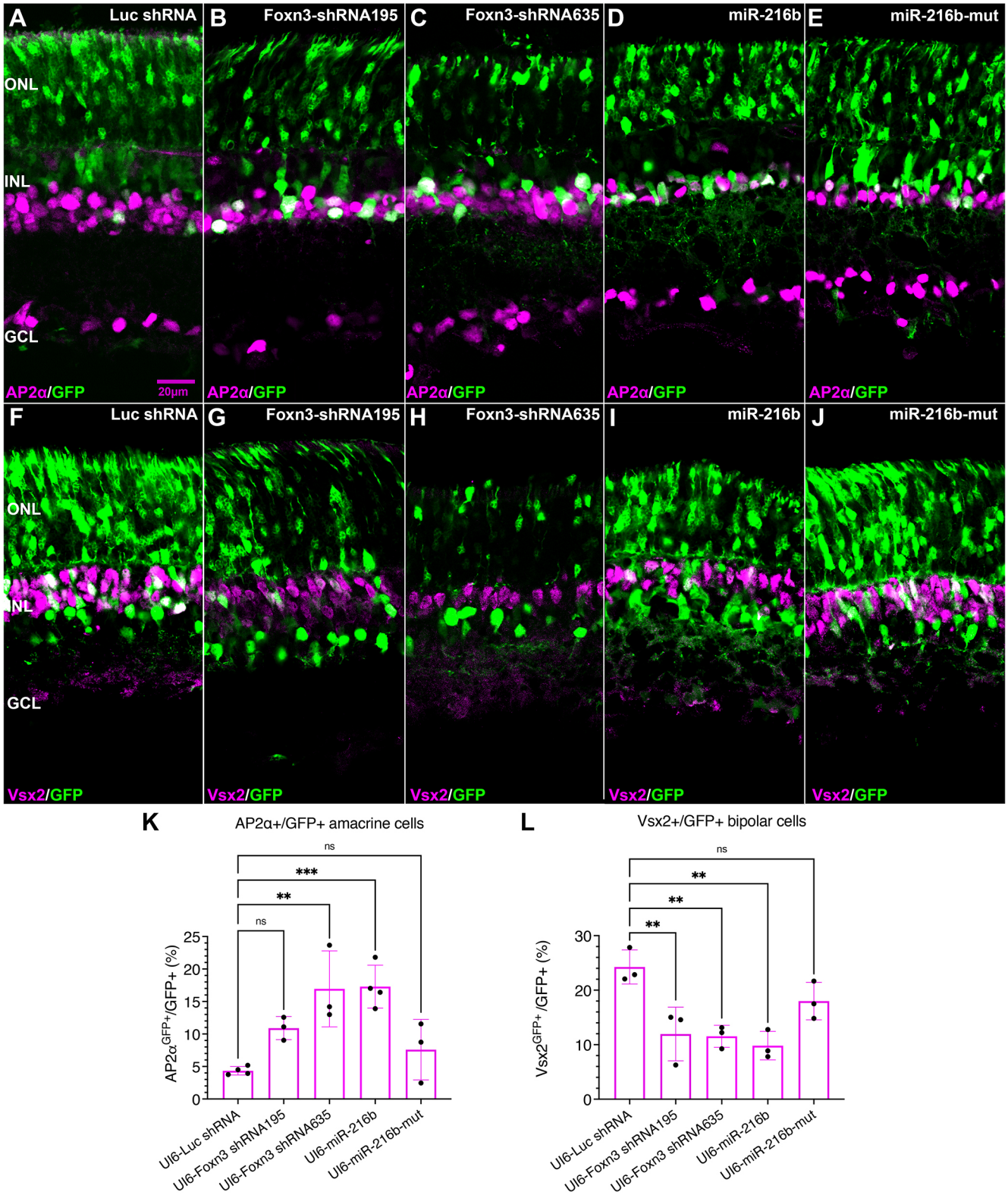

Fig. 5. Foxn3 RNAi increases amacrine cells and reduces bipolar cells, while increased amacrine cell formation after miR-216b expression depends on the miR-216b-5p seed sequence. Plasmid vectors that co-express GFP (green) with shRNAs or miRNAs were introduced into retinas by *in vivo* electroporation at P0; retinas were analyzed at P12. (A-C,K) Expression of one of two shRNAs targeting Foxn3 significantly increased GFP-labeled amacrine cells at P12 relative to the Luc shRNA control vector. (D,E,K) The miR-216b vector increased GFP-labeled amacrine cells (AP2α, magenta) at P12 relative to the control, while a vector expressing GFP and miR-216b-mut did not. (F-J,L) Expression of either Foxn3 shRNA or miR-216b reduced GFP-labeled bipolar cells (Vsx2, magenta), whereas miR-216b-mut did not significantly reduce bipolar cells. Quantitation is shown in K,L. n=3 except n=4 for Luc and miR-216b in K; significance is based on one-way ANOVA with Dunnett's multiple comparisons test: $^{**}P<0.01$, $^{***}P<0.001$; ns, not significant. INL, inner nuclear layer; GCL, ganglion cell layer; ONL, outer nuclear layer. Data are mean±s.d. with individual data points indicated.

Development (2022) 149, dev199484. doi:10.1242/dev.199484

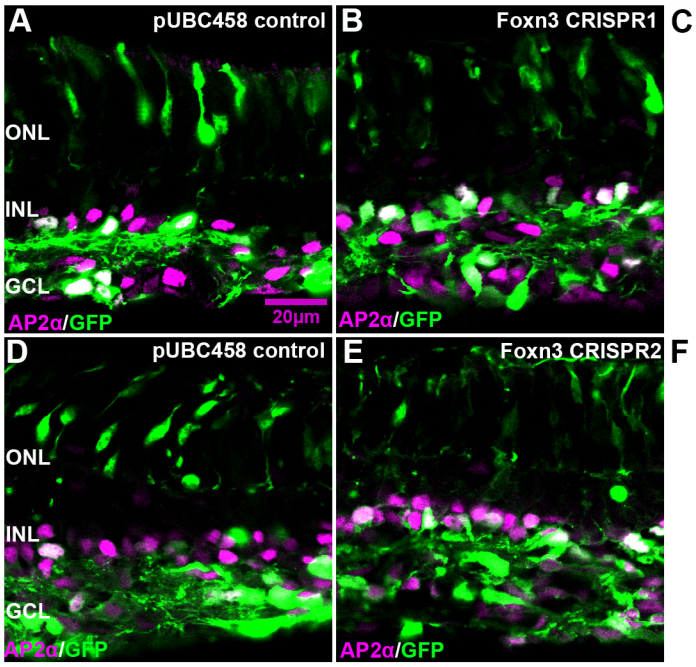

Fig. 6. Disruption of Foxn3 by CRISPR/Cas9 increases amacrine cell formation in embryonic retinal explants. pUBC458 Cas9 or pUBC458 Cas9/Foxn3 sgRNA plasmid expression vectors (see Fig. S9), which co-express Cas9 and GFP, were introduced by electroporation into E16.5 retinas that were maintained in explant culture for 8 DIV. (A-F) Either of two Cas9 vectors with different sgRNAs targeting the Foxn3 gene increased the fraction of amacrine cells (AP2α, magenta) among GFP-labeled cells (green), relative to control vector. Quantitation is shown in C,F. n=4 for control in C, n=3 otherwise; significance is based on a two-tailed, unpaired t-test: *P<0.05, **P<0.01. INL, inner nuclear layer; GCL, ganglion cell layer; ONL, outer nuclear layer. Data are mean±s.d. with individual data points indicated.

electroporation, and then maintained the retinas in explant culture for 2 or 8 DIV. Forced expression of Foxn3 reduced the fraction of AP2α-positive cells among GFP-labeled cells at 8 DIV, relative to a control expression vector (Fig. 7A,B,I). Ptf1a is transiently expressed in newly generated postmitotic amacrine cells (Fujitani et al., 2006). The Foxn3 expression vector reduced the fraction of Ptf1a-positive cells among the GFP-labeled cells at 2 DIV, relative to the control (Fig. 7E-H,K). We also scored cell proliferation/DNA synthesis by incorporation of 5-ethynyl-2′-deoxyuridine (EdU) in the explants at 2 DIV (Zeng et al., 2010). The fraction of GFP-labeled cells that incorporated EdU was significantly increased with the Foxn3 expression vector relative to control (Fig. 7C-D,J). These data indicate that Foxn3 can inhibit amacrine cell formation at an early step, prior to Ptf1a expression and that expression of Foxn3 likely reduces cell cycle exit of retinal progenitor cells.

Co-expression of Foxn3 partially reverses the effects of miR-216b

We tested whether co-expression of the Foxn3 protein could reverse the effects of forced miR-216b expression in the developing postnatal retina. We performed *in vivo* electroporation at P0 to co-deliver the miR-216b and Foxn3 expression vectors individually or together, as well as control vectors, into the retina. We assessed amacrine and bipolar cell markers in GFP-labeled cells at P12 (Fig. 8A-D,I,J). Expression of miR-216b increased the fraction of AP2α amacrine cells and decreased the fraction of $Vsx2^{+}$ bipolar cells among GFP-labeled cells at P12, relative to the Luc shRNA control vector. Co-expression of Foxn3 with miR-216b partially reversed both the increase in amacrine cells and the decrease in bipolar cells among GFP-labeled cells that were observed with expression of miR-216b alone. Expression of Foxn3 by itself in the postnatal retina slightly decreased Vsx2-positive cells among the GFP-labeled cells at P12 but did not significantly decrease AP2α-positive cells. However, we observed an increase in GFP-labeled cells within the INL that were not labeled by either Vsx2 or AP2α when Foxn3 was expressed, with or without miR-216b (Fig. 8K). We scored GFP-labeled cells in the ONL, likely rod photoreceptors based on morphology and lack of Vsx2 or AP2α expression (Fig. 8L). Expression of miR-216b did not significantly change the frequency of GFP-labeled cells in the ONL, although co-expression of Foxn3 and miR-216b slightly decreased the frequency of these cells. Finally, the frequency of Müller glial cells (Sox2 positive/AP2α negative) among the GFP-labeled cells in the INL (Fig. 8E-H,M) did not change significantly with miR-216b, with or without Foxn3. The ability of Foxn3 to partially reverse the effects of miR-216b are consistent with inhibition of Foxn3 as a component of the mechanism by which ectopic expression of miR-216b alters cell type generation in the developing retina.

DISCUSSION

Expression of miR-216b-5p overlaps with differentiated amacrine cells in the mouse retina. miR-216b forms a genomic miRNA cluster with miR-216a and miR-217, two miRNAs expressed from the same primary transcript (Kato et al., 2009). All three miRNAs are expressed in mouse inner retina, consistent with previous observations of miR-216a/miR-217 expression in zebrafish (Olena et al., 2015; Wienholds et al., 2005), and these miRNAs were downregulated in retinas without Ptf1a, a bHLH transcription factor required for the differentiation of nearly all horizontal and amacrine cells. As Ptf1a is transiently upregulated only after amacrine cells become postmitotic (Fujitani et al., 2006), all three miRNAs are preferentially expressed in postmitotic amacrine cells. The lack of high-level expression of these miRNAs in the neuroblast layer of the developing retina, as well as the dependence on Ptf1a, suggest that miR-216a/b are unlikely to regulate initial commitment or cell cycle exit of amacrine cells during retinal development. Nonetheless, ectopic expression of pre-miR-216a or pre-miR-216b in the developing mouse retina led to a significant increase in amacrine cells. The increase in amacrine cells with miR-216b depended on the miR-216b-5p seed sequence, indicating that seed-based target repression by mature miR-216b-5p is likely to drive the increase in amacrine cells. However, expression of miR-216b in retinas in which the Ptf1a gene was disrupted failed to generate amacrine cells, indicating that expression of miR-216b cannot replace Ptf1a. We propose that the normal role of miR-216b and miR-216a is likely to be reducing the expression of repressors of amacrine cell

Development (2022) 149, dev199484. doi:10.1242/dev.199484

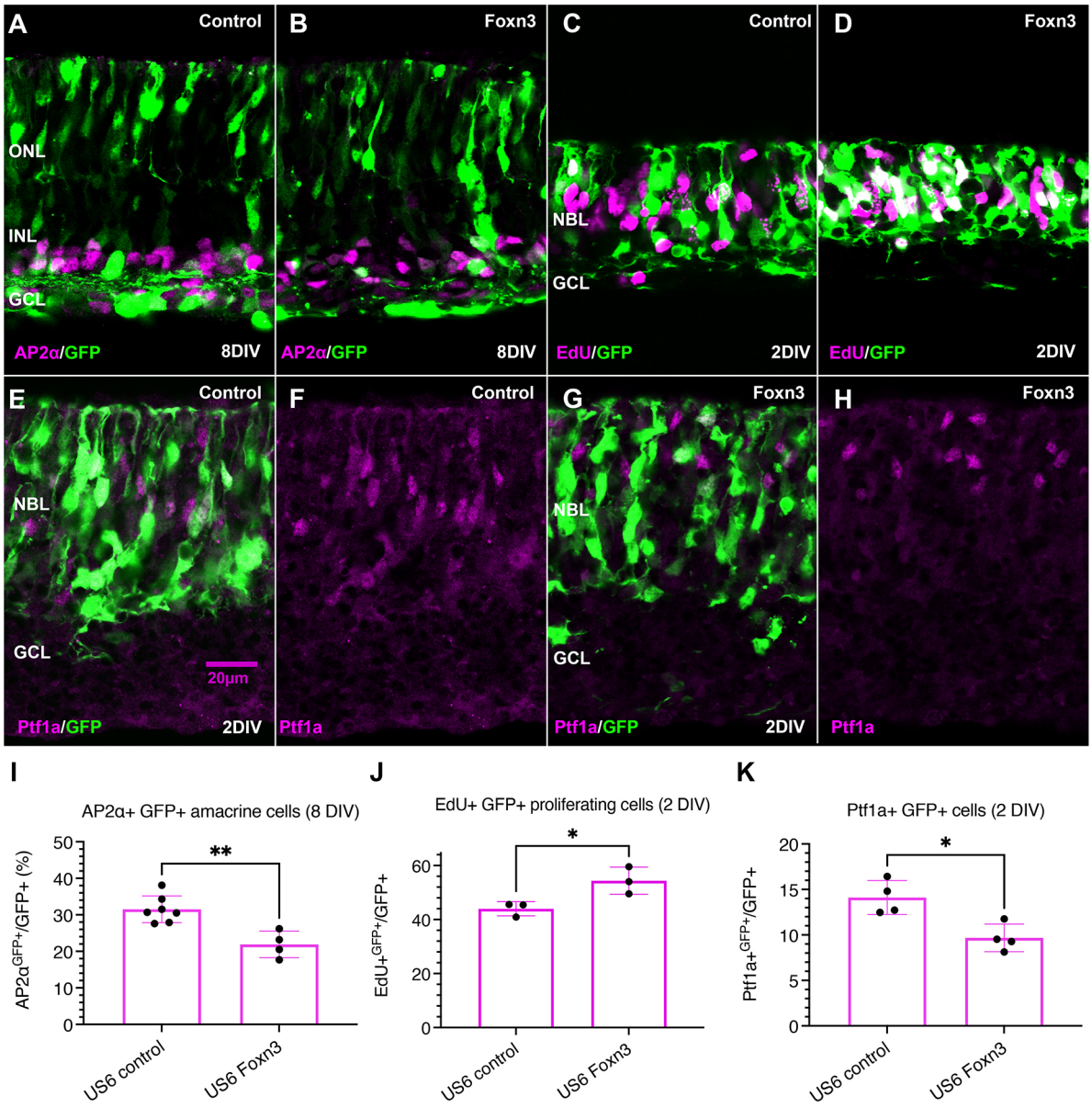

Fig. 7. Ectopic expression of Foxn3 reduces differentiated amacrine cells and increases proliferation in embryonic retinal explants. A GFP expression vector and either a Foxn3 or control expression vector were introduced into E16.5 retinas by electroporation; retinas were then maintained in explant culture. (A,B) Expression of Foxn3 reduced the fraction of amacrine cells (AP2α, magenta) among GFP-labeled cells (green), relative to control vector at 8 DIV. (C,D) Foxn3 expression increased the fraction of GFP-labeled cells in S phase, based on EdU incorporation (magenta) at 2 DIV, relative to control vector. (E-H) Foxn3 also reduced the fraction of GFP-labeled cells that express Ptf1a protein (magenta) at 2 DIV (G,H), relative to the control vector (E,F). Quantitation is shown in I-K. (I) Control, *n*=7; Foxn3, *n*=4; (J) *n*=3; (K) *n*=4. Significance is based on a two-tailed, unpaired *t*-test: **P*<0.05, ***P*<0.01. NBL, neuroblast layer; INL, inner nuclear layer; GCL, ganglion cell layer; ONL, outer nuclear layer. Data are mean±s.d. with individual data points indicated.

differentiation (and possibly other genes) in postmitotic, differentiating amacrine cells, and that ectopic expression of these miRNAs in retinal progenitor cells leads to premature inhibition of their targets and a consequent increase in amacrine cell formation (Fig. 8N,O). A functional requirement for the miR-216a/miR-216b/miR-217 genomic cluster in retinal development has not been evaluated, as the homozygous deletion of the gene cluster in mouse embryos is lethal prior to retina formation (Azevedo-Pouly et al., 2017). However, mice lacking the individual miRNAs are viable, suggesting that miR-216a/b may have redundant roles in embryonic development (Sutaria et al., 2019). A possible association between miR-216a/b sequence variants and inherited retinal disease in humans has been reported (Huang et al., 2018), and miR-216b is upregulated in human retinoblastoma (Ravishankar et al., 2020). In zebrafish, miR-216a regulates sorting nexin 5 (SNX5) during retinal development (Olena et al., 2015), but the miR-216a target sites are not conserved in mouse Snx5. Zebrafish miR-216a also is involved in Müller cell reprogramming during retinal regeneration (Kara et al., 2019).

We identified Foxn3 as a target of miR-216a/b-5p, based on crosslinking of the Argonaute protein by PAR-CLIP near an evolutionarily conserved miR-216a/b-5p seed match in the Foxn3 3′ UTR. We confirmed that miR-216b-5p could repress reporters based on the Foxn3 3′ UTR via two miR-216a/b-5p seed matches.

Development (2022) 149, dev199484. doi:10.1242/dev.199484

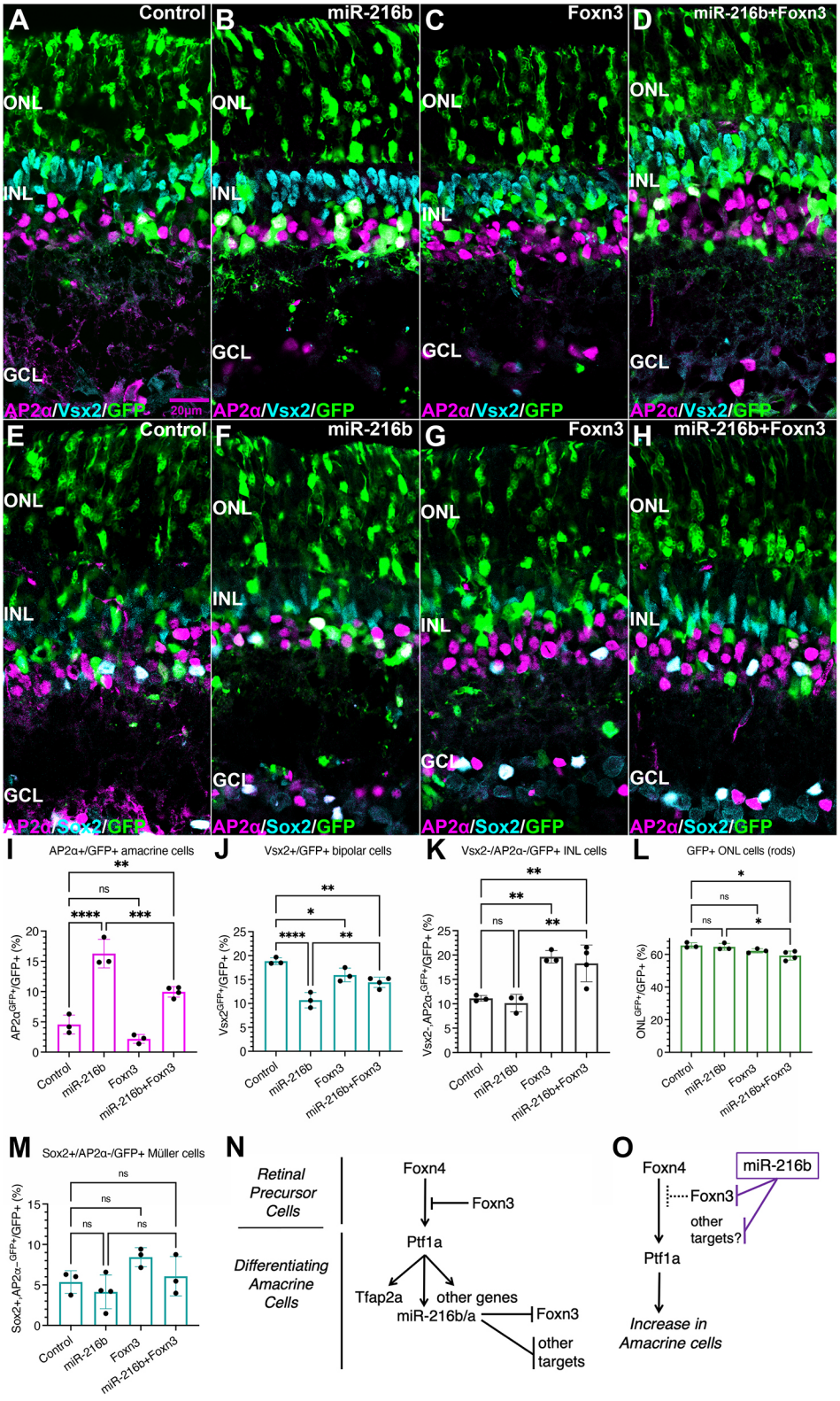

Fig. 8. Co-expression of Foxn3 with miR-216b reduces the effects of miR-216b on amacrine cell and bipolar cell generation in the developing retina. A vector expressing miR-216b and GFP, or a control vector expressing Luc shRNA and GFP, in combination with a Foxn3 or control expression vector, were introduced into retinas at P0 by *in vivo* electroporation. (A-D) GFP-labeled (green) amacrine cells (AP2α, magenta) and bipolar cells (Vsx2, cyan) or (E-H) Müller glia (positive for Sox2, cyan; negative for AP2α, magenta) were assessed at P12; quantitation is shown in I-M. (I,J) The increased fraction of amacrine cells and decreased fraction of bipolar cells among GFP-labeled cells with miR-216b expression were partially reversed by co-expression of Foxn3. (K) Foxn3 expression, with or without miR-216b, increased the fraction of GFP-labeled cells in the INL unlabeled by either AP2α or Vsx2. (L) The fraction of GFP-labeled cells in the ONL (presumptive rod photoreceptors) did not change with miR-216b expression, but was slightly reduced by Foxn3 with miR-216b. (M) GFP-labeled Müller glia fraction did not change significantly with miR-216b and/or Foxn3 expression. (N,O) Proposed models. (N) Foxn3 repression limits amacrine cell formation prior to Pf1a expression; miR-216b represses target mRNAs in differentiating amacrine cells. (O) Ectopic or premature expression of miR-216b in retinal progenitor cells inhibits Foxn3 expression, allowing increased amacrine cell formation driven by Foxn4 (O). (I-L) n=3, except for miR-216b+Foxn3 (n=4). (M) n=3, except for miR-216b (n=4). Significance is based on one-way ANOVA with Holm-Šídák's multiple comparisons test: *P<0.05, **P<0.01, ***P<0.001, ****P<0.0001; ns, not significant. Data are mean±s.d. with individual data points indicated. INL, inner nuclear layer; GCL, ganglion cell layer; ONL, outer nuclear layer.

Foxn3 is widely expressed in the early retina, and, strikingly, inhibition of Foxn3 expression in postnatal retina by RNAi or disruption of the Foxn3 gene by CRISPR/Cas9 in embryonic retinal explants led to an increase in amacrine cell formation, similar to that observed with miR-216b overexpression. Furthermore, ectopic expression of Foxn3 in embryonic retinal explants reduced the frequency of differentiated amacrine cells at 8 DIV. Ectopic Foxn3 also reduced expression of Ptf1a and modestly increased the fraction of proliferating cells in explants 2 days after electroporation, consistent with inhibition of amacrine cell formation at an early step, prior to cell cycle exit. Taken together, these data indicate that Foxn3 is a negative regulator of amacrine cell formation in the

Development (2022) 149, dev199484. doi:10.1242/dev.199484

developing retina, likely limiting the initial formation of amacrine cells. Co-expression of Foxn3 with miR-216b partially reversed the increase in amacrine cell frequency seen with miR-216b expression, suggesting that inhibition of Foxn3 likely contributes to the effects of ectopic miR-216b. However, additional miR-216a/b targets also may contribute to the phenotypes observed after ectopic expression of miR-216a/b. In addition, regulation of Foxn3 by other miRNAs has been described in non-neural cells, including miR-182 (Zhang et al., 2021), a miRNA highly expressed in retina (Xu et al., 2007; Zhuang et al., 2020), and miR-135b (Han et al., 2019), via a site near miR-216a/b site 1 in the Foxn3 3′ UTR. miR-135b-5p is expressed in retina (Table S2), so combinatorial or redundant miRNA regulation of retinal Foxn3 is possible.

Foxn3 has been linked to multiple biological processes, including cell proliferation, epithelial-mesenchymal transition and regulation of glucose metabolism (Huot et al., 2014; Karanth et al., 2018; Li et al., 2017). Reduced Foxn3 function in frogs or mice leads to defects in head neural crest and a small eye phenotype (Samaan et al., 2010; Schuff et al., 2007). We focused on Foxn3 both because a conserved miR-216a/b-5p seed match in the Foxn3 3′ UTR had the most crosslinks among potential miR-216a/b-5p sites in the retina Argonaute PAR-CLIP data, and because Foxn3 is closely related to Foxn4. Foxn4 is a transcription factor expressed in proliferating retinal progenitor cells that is required for amacrine and horizontal cell formation (Li et al., 2004), and this role is evolutionarily conserved (Boije et al., 2013). Foxn4 is a transcriptional activator that directly activates transcription of Ptf1a and other genes (Del Barrio et al., 2007; Liu et al., 2020; Luo et al., 2012). Foxn3 and Foxn4 have been reported to bind to similar DNA target sequences, although Foxn3 also recognizes an additional class of DNA target sequences that Foxn4 does not (Nakagawa et al., 2013; Rogers et al., 2019). As Foxn3 is a transcriptional repressor (Scott and Plon, 2005), we speculate that Foxn3 could bind to and repress direct Foxn4 target genes, thus reducing amacrine cell formation. Consistent with this model, overexpression of Foxn3 reduced the frequency of Ptf1a-positive cells in the developing retina. Alternately, the ability of Foxn3 to recognize binding sites structurally distinct from sites recognized by Foxn4 could allow Foxn3 to regulate other target genes.

Ectopic expression of miR-216b or inhibition of Foxn3 by RNAi significantly reduced the number of retinal bipolar cells among the electroporated retinal cells, whereas co-expressed Foxn3 partially reversed the reduction of bipolar cells by miR-216b. Although clones of mouse retinal cells derived from a single progenitor cell can contain both amacrine and bipolar cells (Turner et al., 1990), the majority of these two cell types are generated at different times during development, with peak amacrine formation near E17 and peak bipolar generation at P1-P3 (Voinescu et al., 2009). Ectopic expression of Foxn4 during retinal development reduces bipolar cell formation (Li et al., 2004). Lineage tracing in Dll4-Cre mice indicates that most or all bipolar cells are generated from retinal progenitor cells that did not express Dll4 (Zou et al., 2015), a direct target of Foxn4 (Luo et al., 2012), suggesting that bipolar cells may arise from progenitor cells in which Foxn4 target genes were not activated. These observations suggest that both increased amacrine cell formation and decreased bipolar cell formation could arise from elevated Foxn4 activity, consistent with a model in which Foxn3 limits Foxn4 function, and miR-216b-5p inhibits Foxn3 expression. We also observed that Foxn3 mRNA is expressed in bipolar cells in the P12 retina, consistent with a role for Foxn3 in bipolar cells. However, overexpression of Foxn3 by itself in postnatal retinas reduced the fraction of bipolar cells relative to control, albeit less than miR-216b, suggesting that Foxn3 can have other effects, directly or indirectly, on bipolar cell formation.

Forced expression of Foxn3 in embryonic retinal progenitor cells did not prevent all amacrine cell formation among electroporated cells. Foxn3 interacts with other proteins (Li et al., 2017; Scott and Plon, 2005), so Foxn3 function could be limited by absence of a co-factor in some cells. Function or stability of Foxn3 protein also could be modulated by post-translational modification, as reported for the related Foxn2 protein (Ma et al., 2018). However, we cannot rule out the possibility that Foxn3 was expressed at an insufficient level in some cells, or that some electroporated cells committed to the amacrine cell fate prior to ectopic Foxn3 expression.

Morphological and molecular analyses have identified numerous subtypes of amacrine cells in mouse retina (MacNeil and Masland, 1998; Macosko et al., 2015; Yan et al., 2020). Based on recent single cell sequencing (Yan et al., 2020), cholinergic amacrine cells express Foxn3 mRNA. It is possible that miR-216a/b limits expression of the Foxn3 protein in cholinergic amacrine cells. As cholinergic amacrine cells are generated prior to E17 (Voinescu et al., 2009), RNAi and CRISPR experiments presented here were too late to reduce Foxn3 expression in those cells.

Transcription of the miR-216a/217 miRNA primary transcript in diabetic kidney cells is activated by TGFβ signaling and bHLH transcription factors (Kato et al., 2009). Intriguingly, amacrine cells express TGFβ2 and the Tgfbr2 receptor (Ma et al., 2007; Tachibana et al., 2016), which could potentially contribute to miR-216a/b/miR-217 upregulation via autocrine signaling. In addition to Ptf1a, the Ascl1, Neurod1 and Neurod4 bHLH proteins are redundantly required for amacrine cell formation (Akagi et al., 2004; Inoue et al., 2002), suggesting that those proteins could regulate transcription of miR-216b/a/miR-217 in the retina. A genome-wide analysis of Ptf1a and Ascl1-binding sites identified ChIP-Seq peaks for Ptf1a and Ascl1, including in the region upstream of the miR-216b miRNA precursor on Chr.11, in cells from mouse spinal cord (Borromeo et al., 2014). In addition, miR-216a/b and miR-217 are highly expressed in mouse pancreas (Azevedo-Pouly et al., 2017; Sutaria et al., 2019), a tissue dependent on Ptf1a function during development, indicating a link between Ptf1a and expression of these miRNA genes in multiple tissues.

Previous analyses of miRNA function in retina have revealed roles in developmental timing. Loss of all miRNAs after disruption of the Dicer processing enzyme can lead to prolonged production of early retinal cell types and loss of later cell types, including amacrine cells (Georgi and Reh, 2010). Other miRNAs also have been implicated in amacrine cell development. We identified miR-181b as another miRNA with elevated expression in mouse amacrine cells that depends on Ptf1a function (Zhuang et al., 2020). In Medaka, retinal miR-181a/b expression depends on TGF-β signaling, and miR-181a/b have been implicated in amacrine and ganglion cell process maturation (Carrella et al., 2015a,b).

Our results identify Foxn3 as a novel regulator of amacrine cell and bipolar formation during mouse retinal development, and they suggest a role for miR-216b in gene regulation in amacrine cells. Both are expected to function as repressors, suggesting that their roles are likely to be to limit expression of other regulators. Multiple repressive factors, such as Prdm1 and Vsx2, regulate bipolar cell and amacrine cell formation (Goodson et al., 2020), as well as additional, unidentified transcriptional repressors in bipolar or Müller cells (Chan et al., 2020). Identification of targets of Foxn3 in retina should help to decipher regulatory networks that control cell diversification in the developing retina.

Development (2022) 149, dev199484. doi:10.1242/dev.199484

MATERIALS AND METHODS

Plasmid construction

Plasmids were constructed using standard techniques. Oligonucleotides and gBlocks used for plasmid construction are listed in Table S7. The pUS2, pUS2-MT, pUS2-eGFP, pUS2-Puro, pUS2-Luc, pUI4-GFP-SIBR, pUI4 Luc-shRNA (Chung et al., 2006) and pUS2-Tol2 transposase (Gupta et al., 2018) have been described previously. The pUS6, pUI6-GFP-SIBR and pUI6 Luc-shRNA plasmids are variants of pUS2, pUI4-GFP-SIBR and pUI4 Luc-shRNA that have ITRs from the Tol2 transposon flanking the expression cassettes to allow for integration in the presence of Tol2 transposase (Balciunas et al., 2006). Partial primary transcript sequences (pre-miRNAs and some flanking sequences) for the mouse miR-216a, miR-216b and miR-217 genes were amplified by PCR from mouse genomic DNA and cloned into pUI4-GFP-SIBR and pUI6-GFP-SIBR using primers with the indicated restriction sites. Pre-miR-216b-mut, with a 3 nt mutation in the seed sequence of miR-216b-5p (AATCTCT to AATAGAT) and a compensating change in miR-216b-3p to maintain base pairing in the pre-miRNA, was synthesized as a gBlock (IDT) and inserted into pUI6-GFP-SIBR. The mouse Foxn3- and Foxn4-coding regions were isolated by RT-PCR from embryonic mouse retina RNA and inserted into pUS2 and pUS6. Foxn3 shRNA constructs pUI6-GFP-SIBR Foxn3-195×2 and pUI6-GFP-SIBR Foxn3-635×2 contain two tandem miR-155-based SIBR cassettes (Chung et al., 2006), which target the coding region of the mouse Foxn3 mRNA. The NanoLuc coding region was PCR amplified from plasmid pNL.1.1 (Promega) and inserted into pUS2-MT to generate pUS2-MT-Nanoluc. The Foxn3 3′UTR 1-266 fragment (first base of Foxn3 stop codon is position 1) containing wild-type or mutated miR-216a/b target sites (mutated site sequences altered to match the seed sequence of miR-216b-mut) were generated by RT-PCR from mouse retina RNA, then inserted downstream of firefly Luciferase in pUS2-Luc. The remaining Foxn3 3′ UTR and presumptive endogenous polyadenylation site were amplified from mouse genomic DNA, then inserted into the Foxn3 3′ UTR 1-266 luciferase reporter plasmid DNA using the NEBuilder HiFi DNA Assembly Cloning Kit (New England Biolabs). pUBC458 was made by replacing CBH promoter in pX458 (AddGene #48138) (Ran et al., 2013) with the human UBC promoter and first intron from pUI4-GFP-SIBR (Chung et al., 2006), followed by replacement of the original sgRNA scaffold with an optimized sgRNA scaffold (Dang et al., 2015) to make pUBC458op, both plasmids retaining the U6 promoter and Bbs1 cloning sites from pX458. Oligonucleotides for Foxn3 sgRNAs were designed using E-CRISP (Heigwer et al., 2014) and inserted into pUBC458 (Foxn3 CRISPR1) or pUBC458op (Foxn3 CRISPR2). A second U6 sgRNA expression cassette was inserted adjacent to the existing U6-sgRNA cassette to express two sgRNAs.

Mice and processing of retinas

All mouse (*Mus musculus*) experiments were approved by the Institutional Animal Care & Use Committee at the University of Michigan. Wild-type retinas were isolated from CD-1 mice of both sexes (Charles River). *Ptf1a* mutant mice have the *Ptf1a*-coding region replaced with the *Cre*-coding region (Kawaguchi et al., 2002). Eyes were fixed with 2% paraformaldehyde (ThermoFisher) in phosphate-buffered saline (PBS, Sigma) for 30 min at room temperature, retinas were dissected from the eyes, then cryoprotected in PBS containing 30% sucrose (Sigma) for 2 h at 4°C, and embedded in OCT (Sakura), prior to preparation of cryosections (16 µm) using a cryostat. All the retinas were processed similarly to obtain tissue for either *in situ* hybridization or antibody staining.

In vivo and *in vitro* electroporation, and retina explant culture

1 µl of plasmid DNA vectors were injected into the subretinal space of P0 mouse pups and introduced into cells by *in vivo* electroporation as described previously (Zhang et al., 2012). The concentration and combination of DNA vectors are listed below. 2 µg/µl pUI4 miRNA expression vectors or pUI4 Luc-shRNA control (Fig. 2), or 2 µg/µl pUI6 miR-216b expression vector, 2 µg/µl pUI6 miR-216b-mut, 2 µg/µl pUI6 Luc-shRNA or 2 µg/µl pUI6 Foxn3 RNAi vectors, and 200 ng/µl pUS2-Tol2 were injected (Fig. 5). 2 µg/µl pUI6 miR-216b expression vector or 2 µg/µl pUI6 Luc-shRNA, and 1 µg/µl pUS6-Foxn3 expression vector or 1 µg/µl pUS6 control, and 300 ng/µl pUS2-Tol2 were injected in Fig. 8. After DNA injection, five square 80 V pulses of 50 ms duration with 950 ms intervals were applied by using an ECM830 (BTX) with forcep-type electrodes. Electroporated retinas were collected at P7 (Fig. 2) or P12 (Figs 5 and 8).

For retinal explants, heads from E16 mouse embryos were split in half along the sagittal suture and the cut surface of the tissue was placed on a square plate electrode. Plasmids were introduced into retinal cells by *in vitro* electroporation. 0.5 µl of plasmid DNA vectors were injected into the subretinal space of each eye. 2 µg/µl of pUBC458/pUBC458op Foxn3 CRISPR vectors or pUBC458/pUBC458op control (Fig. 6), 2 µg/µl pUI6 miR-216b or pUI6 Luc shRNA expression vectors and 200 ng/µl pUS2-Tol2 (Fig. S4), or 1 µg/µl pUS6 or pUS6-Foxn3 overexpression vector combined with 1 µg/µl pUS6-GFP expression vector and 200 ng/µl pUS2-Tol2 (Fig. 7) were injected. After DNA injection, five square 30-V pulses of 50 ms duration with 950 ms intervals were applied by using an ECM830 (BTX) with a platinum needle electrode above the eye in combination with the plate electrode underneath the embryonic tissue (Matsuda and Cepko, 2004). Electroporated retinas were dissected from the eyes, placed in six-well plates on Transwells with polyester membrane (Corning, pore size 0.4 µm), the ganglion cell layer facing upwards, and cultured in 1.2 ml of high-glucose Dulbecco's modified Eagle's medium (DMEM) supplemented with 20% horse serum and 1% penicillin-streptomycin (all Thermofisher). Retinas were collected 2 or 8 days after electroporation.

In situ hybridization and immunofluorescence

miRNAs *in situ* hybridization with alkaline-phosphatase detection by BCIP/NBT was performed as described previously (Deo et al., 2006; Zhuang et al., 2020). RNA oligonucleotide probes were synthesized with both 5′ and 3′ fluorescein modifications (Sigma) and gel purified. Sequences of oligoribonucleotide probes are in Table S7. For fluorescent detection of miRNA *in situ* hybridization, the same method was used until the alkaline-phosphatase detection step. After the alkaline-phosphatase conjugated anti-fluorescein Fab2 antibody (Roche, 11426338910) was removed, slides were washed twice in 1× Tris-buffered saline (Thermofisher) (Zhuang et al., 2020) for 10 min each. A Fast Red tablet (Sigma) was reconstituted in water according to the manufacturer's instructions and 200 µl Fast Red solution was added to each slide at room temperature. Slides were monitored closely, and staining was stopped by washing the slides in PBS.

mRNA *in situ* hybridization with RNA probes was performed as described previously (Deo et al., 2006; Zhang et al., 2012). Restriction enzyme linearized plasmid pUS2-Foxn3 or pUS2-Foxn4 was used as template for the synthesis of UTP-fluorescein or UTP-digoxigenin (Roche) labeled riboprobes by *in vitro* transcription. For split initiator mRNA *in situ* hybridization chain reaction (HCR) (Choi et al., 2018), Foxn3 or Foxn4 mRNA was hybridized with a pool of 20 probe pairs (IDT), and detected using matching 72 nt hairpin HCR amplifiers (Molecular Technologies). Detailed protocols for mRNA *in situ* HCR were described previously (Zhuang et al., 2020). Sequences of *in situ* HCR probes are in Table S7.

Indirect immunofluorescence analysis was performed on retinas without *in situ* hybridization or after *in situ* hybridization. For AP2α antibody staining, retina sections were blocked with 1:400 unlabeled affinity-purified Fab fragment donkey anti-mouse IgG (H+L) (Jackson Immunoresearch, 715-007-003) and 5% donkey serum (Thermofisher) in PBS with 0.05% Triton X-100 (Thermofisher) at 4°C overnight, incubated with mouse anti-AP2α (1:1000, Developmental Studies Hybridoma Bank, 3B5), then incubated with Alexa Fluor 647-conjugated or Alexa Fluor 546-conjugated anti-mouse secondary antibody (both 1:1000, Jackson Immunoresearch, 715-605-051) for 1 h at room temperature. For Vsx2 (Chx10), Ptf1a, Sox2 and GFP staining, tissue sections were blocked with 5% donkey serum, and incubated with sheep anti-Chx10 (1:100, Millipore, AB9016), rabbit anti-Ptf1a (1:800, Li and Edlund, 2001), rabbit anti-Sox2 (1:1000, Millipore, AB5603) or chick anti-GFP (1:500, Aves Labs, GFP-1020) at 4°C overnight, followed by incubation with Alexa 594-conjugated anti-sheep secondary antibody, Alexa 594-conjugated anti-rabbit secondary antibody or Alexa 488-conjugated anti-chick secondary antibody (1:1000, Jackson Immunoresearch, 713-585-147, 711-585-152 and 703-545-155). After antibody staining, Hoechst 33342 (Roche) was used to stain nuclei. For EdU

Development (2022) 149, dev199484. doi:10.1242/dev.199484

labeling, retinal explants were incubated with EdU for 12 h prior to collection, then the Click-iT EdU Cell Proliferation kit (ThermoFisher) was used to detect EdU, as directed by the manufacturer.

Microscopy and imaging

BCIP/NBT staining was imaged with a Leica DSMIRB microscope with a SPOT-RT digital camera or a Zeiss Axiovert microscope with an AmScope MU-2003-BI camera. Fluorescent antibody staining with GFP or *in situ* hybridization/HCR were imaged using an Olympus FV1000 confocal microscope. Images were analyzed and colors were assigned with FV10-ASW 3.1 Viewer or FIJI/ImageJ. Representative images were cropped, assembled and labeled using Adobe Photoshop.

Cell counts, graphs and statistics

GFP^+/antibody-positive cells were analyzed from at least three retinas for each condition. Cells were counted manually from images, and analysis was not masked because, for most experiments, altered cell numbers among the GFP-labeled cells in specific retinal layers were discernible by eye prior to counting. Cell counts were totaled across several sections for each sample. The range for the number of GFP+ cells counted per vector (all samples combined) in each figure: 1516-2587 (Fig. 2), 1898-2511 (Fig. 5), 1529-3029 (Fig. 6), 1962-2070 (Fig. 7I), 648-738 (Fig. 7J), 1527-1606 (Fig. 7K), 1937-3570 (Fig. 8I-L) and 2345-3356 (Fig. 8M). Error bars show standard deviation for all graphs. For qRT-PCR in Fig. 1B, one-tailed *t*-tests were used. For cell count graphs, two tailed *t*-tests were used for pairwise comparisons, whereas multiple comparisons were analyzed by one-way ANOVA with Dunnett's multiple comparisons test or Holm-Šídák's multiple comparisons test. Luciferase reporter assays in Fig. 4 were analyzed by two-way ANOVA with Tukey's multiple comparisons test. Graph generation and statistical analysis were performed with GraphPad Prism 9 or Microsoft Excel. The Fig. 3A pie chart was made with DataGraph (Visual Data Tools).

qRT-PCR

PCR primers are listed in Table S7. RNA was extracted from retinas using TRIzol (ThermoFisher) and treated with RNase-free DNaseI (Promega). For miRNA qRT-PCR, 1 µg of RNA was polyadenylated using a Poly (A) Tailing Kit (Thermofisher). After re-purification with TRIzol reagent, total RNA was reverse-transcribed with 0.5 µg of poly (T) adaptor containing a 5′-end universal tag sequence and SuperScript II Reverse Transcriptase (Thermofisher). Specific miRNA primers, in combination with a universal reverse primer that binds to the universal tag sequence, were used to amplify specific miRNA sequences (Thomson et al., 2006). For mRNA qRT-PCR, 1 µg of RNA was reverse transcribed using Superscript II and random 12mer primers. 2.5 ng of cDNA for miRNA assay, or 20 ng of cDNA for mRNA assay was used per real-time PCR with SYBR Green (Bio-Rad) to detect DNA, using a BioRad iCycler with MyiQ light module. Expression of Foxn3 mRNA was normalized to GAPDH mRNA. Data presented are mean of three RNA samples for each condition, each assayed using triplicate PCR replicates. The $2^{-\Delta\Delta CT}$ method was used to calculate fold change.

Transfections, luciferase assays and cell culture RNA collection

HEK293 (Takara Bio) and P19 cells tested negative for mycoplasma. In 24-well plates, HEK293 cells were grown in DMEM with 10% fetal bovine serum (FBS), 100 units/ml penicillin and 100 µg/ml streptomycin (all ThermoFisher). For 266 nt UTR reporter assay, 50 ng pUS2-Luc, pUS2-Luc-Foxn3-UTR-WT, pUS2-Luc-Foxn3-UTR-3′-216b-mutant, pUS2-Luc-Foxn3-UTR-5′-216b-mutant or pUS2-Luc-Foxn3-UTR-5′+3′-216b-mutant was co-transfected with 600 ng of pUI6, pUI6-miR-216b or pUI6-miR-216b-mutant for each well. For full-length UTR reporter assay, 50 ng pUS2-Luc, 100 ng pUS2-Luc-Foxn3-UTR-WT-full length or 100 ng pUS2-Luc-Foxn3-UTR-5′+3′-216b-mutant-full length was co-transfected with 250 ng of pUI6, pUI6-miR-216b or pUI6-miR-216b-mutant for each well. 25 ng of pUS2-MT-Nanoluc was included for each well as an internal control for transfection efficiency. Transfections were performed with Lipofectamine 2000 (ThermoFisher) according to the manufacturer's instructions. Reporter activity was assayed 48 h after transfection using the Bright-Glo and Nano-Glo Luciferase Assay kits (Promega). Firefly Luciferase activity was normalized to Nanoluciferase activity to control for transfection efficiency. A FLUOstar OPTIMA plate reader was used to measure luminescence intensity. Relative expression data shown in Fig. 4 are from six independent transfections. Each transfection sample was analyzed by duplicate (technical replicate) luciferase assays: graph data points show mean of the assay replicates.

Mouse P19 cells were grown in MEM-α with 2.5% FBS, 7.5% calf serum and 1:100 penicillin-streptomycin (all ThermoFisher) (Farah et al., 2000). To determine the effectiveness of Foxn3 RNAi constructs in P19 cells, 3 µg of Foxn3 RNAi vectors and 1 µg of pUS2-Puro were co-transfected into one well of a 6-well plate. Transfections were performed with TransIT-LT1 Transfection Reagent (Mirus) according to the manufacturer's instructions. The transfected cells were shifted to medium with 12.5 µg/ml puromycin (Sigma) 8 h after transfection and selected for 16 h. Total RNA was extracted by using TRIzol 48 h after transfection.

PAR-CLIP libraries

Argonaute PAR-CLIP libraries were prepared based on the method described by Hafner et al. (2010), with modifications based in part on tissue processing used for HITS-CLIP (Chi et al., 2009). P0 retinas from CD-1 mice were isolated and grown as explants for 24 h in high-glucose DMEM supplemented with 20% horse serum and 0.1 mM 4-thiouridine (Sigma). Six retinas were used to make one library. Live, intact retina explants were irradiated with 365 nm UV light (~300 mJ/cm^2) using a Stratalinker (Stratagene), then lysed in 300 µl of low-salt lysis buffer [50 mM HEPES (pH 7.5), 50 mM KCl, 0.5% sodium deoxycholate, 0.1% SDS, 0.5% NP-40, 0.5 mM DTT and Protease inhibitor cocktail (Sigma)] with 6 µl of RNaseout (Life Technologies). The lysates were sequentially treated with 12.6 µl of RNase-free DNase (Promega) and 7.5 µl of 1:1330 diluted micrococcal nuclease (11.3 gel units, New England Biolabs: NEB) for 5 min at 37°C. 8.4 µl of 0.5 M EGTA (Sigma) was added to stop the micrococcal nuclease digestion. Lysates were cleared by centrifugation at 16,000 ***g*** for 10 min at 4°C. Cleared lysates were incubated with 10 µg of 2A8 anti-Argonaute1-4 antibody (EMD-Millipore MABE56) (Nelson et al., 2007) or G3A1 mouse IgG1 isotype control antibody (Cell Signaling Technologies #5415) bound to Protein G Dynabeads (Life Technologies) and rotated at 4°C overnight. Beads were washed three times in IP wash buffer [50 mM HEPES (pH 7.5), 300 mM KCl, 0.5% NP-40, 0.5 mM DTT and Protease inhibitor cocktail], three times in high-salt wash buffer [50 mM HEPES (pH 7.5), 500 mM KCl, 0.5% NP-40, 0.5 mM DTT and Protease inhibitor cocktail] and resuspended in dephosphorylation buffer [100 mM NaCl, 50 mM Tris-HCl (pH 7.9) and 10 mM $MgCl_2$]. 4 µl of calf intestinal alkaline phosphatase (NEB) was added to dephosphorylate the RNA for 15 min at 37°C. Beads were washed twice in phosphatase wash buffer [50 mM Tris-HCl (pH 7.5), 20 mM EGTA, 0.5% NP-40] and twice in polynucleotide kinase (PNK) buffer [50 mM Tris-HCl (pH 7.5), 50 mM NaCl, 10 mM $MgCl_2$]. Beads were resuspended in 80 µl of PNK buffer with 5 mM DTT, and incubated with 8 µl of T4 Polynucleotide Kinase (NEB) and 2 µl of 10 mM ATP for 30 min at 37°C. The beads were washed five times in PNK buffer. The protein-RNA complexes were eluted in 30 µl of 1×Novex Tris-glycine SDS sample buffer (Life Technologies) and separated by 10% SDS-PAGE. A gel slice corresponding to 100 to 150 kDa was isolated (based on size markers in an adjacent lane; Precision Plus Protein Dual Color Standards from Bio-Rad). The gel slice was transferred to a D-Tube Dialyzer Midi Tube (EMD-Millipore). The protein-RNA complexes were electroeluted in 1× NuPage MOPS SDS running buffer (Life Technologies) at 100 V for 2.5 h. The eluate was digested in 50 mM Tris-HCl (pH 7.5), 72 mM NaCl, 6 mM EDTA, 1 mM SDS and 1.2 mg/ml Proteinase K (Sigma) at 55°C for 30 min. RNA was recovered by acidic phenol/chloroform (Life Technologies) extraction and ethanol (Thermofisher) precipitation. The recovered RNA was used to prepare a cDNA library using a TruSeq Small RNA Library Preparation Kit (Illumina) according to the manufacturer's directions, with the following modification: after reverse transcription, the reaction was denatured, separated on a 10% TBE urea gel (Life Technologies); a gel slice corresponding to 80 to 150 nt was isolated (based on size markers in an adjacent lane: low range ssRNA

Development (2022) 149, dev199484. doi:10.1242/dev.199484

ladder, NEB). The reverse transcribed product in the gel slice was eluted, precipitated by adding 2-propanol, suspended in Tris-HCl buffer, then used in subsequent steps. PAR-CLIP libraries were sequenced on an Illumina HiSeq 2500 (University of Michigan Advanced Genomics Core).

Single-end read PAR-CLIP cDNA sequences were mapped to the mouse mm10 genome using STAR (Dobin and Gingeras, 2016). Sequences mapping to ChrM or rRNA sequences were removed. Multiple reads with identical sequence and length were considered duplicates and only a single read was retained. We considered sequence as well as length to avoid discarding potentially identical cDNA fragments with crosslinks at different positions, although this meant that duplicate reads with distinct errors introduced during the PCR amplification of the library would be considered as separate reads. T to C sequence substitutions relative to the genome were identified with Bambino (Edmonson et al., 2011). Reads with low base quality mismatches or near the ends of reads were filtered, so the count of T to C substitutions and coverage at a specific position is conservative (both crosslink counts and read coverage at crosslink sites exclude some input sequences due to filters). T to C substitutions present at the same genomic position in at least two of the five Argonaute PAR-CLIP libraries, but not detected in the two IgG control libraries, were identified, combined and filtered using scripts, BEDtools (Quinlan, 2014) and an in-house program. Reads with small deletions at the same position as a consistent T to C substitution also were considered crosslinked reads. Consistent crosslinks within 15 nt of a position with a greater number of reads with a consistent crosslink were removed, to create the set of predominant crosslinks. Predominant crosslink sites were annotated using GENCODE VM16 gene/exon annotations (Frankish et al., 2019) and BEDTools. 6 or 7 nt miRNA seed matches with the 5′ base of the match within ±15 nt of a predominant crosslink site (31 nt windows) were identified, based on seeds from miRNAs detected in P0 retinas (Table S2). To identify evolutionary conservation of miRNA seed sites, PhastCons (Siepel et al., 2005) scores were determined for both the 31 nt window and individual seed matches at each predominant crosslink, based on the mm10 MAF60 alignment. In addition, sequences corresponding to the seed sequences from several selected species were retrieved via hg19 MAF100 multiple alignments, using Galaxy (Afgan et al., 2018) at the public server usegalaxy.org. The subset of predominant crosslinks that had a 6 or 7 nt match to the miR-216a and/or miR-216b seed sequences in the genome were selected for further analysis. Plots of read coverage were generated using IGV (Thorvaldsdottir et al., 2013).

To evaluate miRNA seed enrichment near predominant crosslinks (Fig. S5), 3′ UTR exons with crosslinks were identified. Overlapping exons on the same strand were merged, and crosslinks near the ends of exons were filtered to avoid seed matches outside the exons. All seed matches within ±15 nt were counted. If overlapping matches were possible for the same seed match, only the longest match was counted. To determine the expected distribution of miRNA seeds near crosslink positions, a Monte-Carlo method was used. Randomly selected Ts from the same set of exons were used as pseudo-crosslinks (same number of pseudo-crosslinks selected per exon as predominant crosslinks identified for that exon, with same filters on position). Seed matches were counted within ±15 nt of the pseudo-crosslinks, for 100,000 trials. Bonferonni correction was used to adjust *P*-values for multiple testing.

Small RNA libraries

Retinas from individual E18.5 embryos (Ptf1a knockout or heterozygous) were isolated and pooled. The genotype of embryos was determined by PCR using the primers: Ptf1a-F, CGAGGACAACGTCAGCTATTG; Ptf1a-R, TCTCGCACATTAGCGGCTTG; Cre-F, CATGCTTCATCGTCGGTCC; and Cre-R, GATCATCAGCTACACCAGAG. Total RNA was purified by using TRIzol, then denatured and separated on a 15% TBE urea gel (Life Technologies). Small RNA was recovered from a gel slice corresponding to ∼18-30 nt (based on size markers in an adjacent lane: 20/100 Ladder, IDT). The gel purified small RNA from 1 µg of total RNA was used to prepare a small RNA library using a NEB Next Multiplex Small RNA Library Prep Kit (New England Biolabs), according to the manufacturer's directions, with the following modification: after reverse transcription, the reaction was denatured, separated on a 10% TBE urea gel; a gel slice corresponding to 60 to 80 nt was isolated (based on size markers in an adjacent lane: low range ssRNA ladder, NEB). The reverse transcribed product in the gel slice was eluted, precipitated by adding 2-propanol (Thermofisher), suspended in Tris-HCl buffer and then used in subsequent steps. Small RNA libraries were sequenced on an Illumina HiSeq 2500 (University of Michigan Advanced Genomics Core). Insert sequences had adaptor sequences trimmed and inserts <18 nt or >30 nt were removed. Sequences were then mapped to mature miRNA sequences in miRBase 22 (www.mirbase.org) (Kozomara et al., 2019) using a custom Python script (https://github.com/daimh/microRNA). Unmapped sequences were discarded. Counts for sequences with equivalent mappings to multiple miRNA sequences were divided among the matches. Counts for each mature miRNA were normalized to input library sizes. We also determined the most frequent sequence for each mature miRNA. Small RNA libraries from P0 CD-1 mouse retinas were made and analyzed by a similar protocol, except that the TruSeq Small RNA Library Preparation Kit (Illumina) was used for library preparation and miRNA sequences were mapped to miRBase 21.

Analysis of single cell RNA-seq data

Published amacrine cell single cell RNA-seq data (Yan et al., 2020) was downloaded from NCBI GEO (GSE149715) and used to generate a gene expression table with normalization and batch correction using the Seurat package (https://satijalab.org/seurat/) as described previously (Yan et al., 2020). Pearson correlation of Foxn3 expression with the other 18,204 genes passing Seurat filtering (Table S5) was performed using R cor.test.

CRISPR sequencing analysis

Genomic DNA was prepared from GFP-positive CD-1 E16 retina explants 48 h after electroporation with either a Foxn3 CRISPR vector or the control vector. Genomic DNA from two pooled explants was purified by using DNeasy Blood & Tissue Kit (Qiagen) for each sample. Q5 high-fidelity DNA polymerase (NEB) was used to PCR amplify genomic DNA at each Cas9 target site. PCR primers are listed in Table S7. PCR products were gel purified, then analyzed by Illumina sequencing at the Massachusetts General Hospital CCIB DNA Core. Sequence reads were analyzed using the online version of CRISPResso2 (Clement et al., 2019).

Acknowledgements

We thank colleagues who generously provided reagents: Marina Pasca di Magliano and Chris Wright for Ptf1a mutant mice, Helena Edlund for anti-Ptf1a antibody, and Mike Uhler for plasmids. We thank Tom Glaser, Brenda Bass, David Chen, Robert Thompson, Anne Vojtek, Beth Rousseau, Robert Davis and Mike Uhler for helpful discussions. This work used the Vision Research Core at the University of Michigan Kellogg Eye Center, supported by the National Institutes of Health (P30EY007003).

Competing interests

The University of Michigan has a patent on miR-155 based RNAi technology. D.L.T. is a recipient of royalties paid to the University of Michigan for licensed use.

Author contributions

Conceptualization: D.L.T.; Methodology: H.Z., P.Z., F.M., D.L.T.; Software: M.D., F.M., D.L.T.; Formal analysis: H.Z., P.Z., F.M., D.L.T.; Investigation: H.Z., P.Z., R.M.W.; Writing - original draft: H.Z., D.L.T.; Writing - review & editing: H.Z., P.Z., R.M.W., F.M., D.L.T.; Visualization: H.Z., P.Z.; Supervision: D.L.T.; Funding acquisition: D.L.T.

Funding

This work was supported by the National Institutes of Health (R01EY024996 and R21EY018707), by the Midwest Eye-Banks (Eversight), and by the University of Michigan Biomedical Research Council and Office of Research (D.L.T.). Deposited in PMC for release after 12 months.

Data availability

PAR-CLIP and small RNA-sequencing data have been deposited in GEO under accession number GSE165832.

Peer review history

The peer review history is available online at https://journals.biologists.com/dev/article-lookup/doi/10.1242/dev.199484.

References

Afgan, E., Baker, D., Batut, B., van den Beek, M., Bouvier, D., Cech, M., Chilton, J., Clements, D., Coraor, N., Grüning, B. A. et al. (2018). The Galaxy platform for accessible, reproducible and collaborative biomedical analyses: 2018 update. *Nucleic Acids Res.* **46**, W537-W544. doi:10.1093/nar/gky379

Akagi, T., Inoue, T., Miyoshi, G., Bessho, Y., Takahashi, M., Lee, J. E., Guillemot, F. and Kageyama, R. (2004). Requirement of multiple basic helix-loop-helix genes for retinal neuronal subtype specification. *J. Biol. Chem.* **279**, 28492-28498. doi:10.1074/jbc.M400871200

Azevedo-Pouly, A. C. P., Sutaria, D. S., Jiang, J., Elgamal, O. A., Amari, F., Allard, D., Grippo, P. J., Coppola, V. and Schmittgen, T. D. (2017). miR-216 and miR-217 expression is reduced in transgenic mouse models of pancreatic adenocarcinoma, knockout of miR-216/miR-217 host gene is embryonic lethal. *Funct. Integr. Genomics* **17**, 203-212. doi:10.1007/s10142-016-0512-1

Balciunas, D., Wangensteen, K. J., Wilber, A., Bell, J., Geurts, A., Sivasubbu, S., Wang, X., Hackett, P. B., Largaespada, D. A., McIvor, R. S. et al. (2006). Harnessing a high cargo-capacity transposon for genetic applications in vertebrates. *PLoS Genet.* **2**, e169. doi:10.1371/journal.pgen.0020169

Bartel, D. P. (2018). Metazoan microRNAs. *Cell* **173**, 20-51. doi:10.1016/j.cell.2018.03.006

Bassett, E. A., Pontoriero, G. F., Feng, W., Marquardt, T., Fini, M. E., Williams, T. and West-Mays, J. A. (2007). Conditional deletion of activating protein 2α (AP-2α) in the developing retina demonstrates non-cell-autonomous roles for AP-2α in optic cup development. *Mol. Cell. Biol.* **27**, 7497-7510. doi:10.1128/MCB.00687-07

Boije, H., Shirazi Fard, S., Ring, H. and Hallböök, F. (2013). Forkheadbox N4 (FoxN4) triggers context-dependent differentiation in the developing chick retina and neural tube. *Differentiation* **85**, 11-19. doi:10.1016/j.diff.2012.12.002

Borromeo, M. D., Meredith, D. M., Castro, D. S., Chang, J. C., Tung, K.-C., Guillemot, F. and Johnson, J. E. (2014). A transcription factor network specifying inhibitory versus excitatory neurons in the dorsal spinal cord. *Development* **141**, 2803-2812. doi:10.1242/dev.105866

Carrella, S., Barbato, S., D'Agostino, Y., Salierno, F. G., Manfredi, A., Banfi, S. and Conte, I. (2015a). TGF-β controls miR-181/ERK regulatory network during retinal axon specification and growth. *PLoS ONE* **10**, e0144129. doi:10.1371/journal.pone.0144129

Carrella, S., D'Agostino, Y., Barbato, S., Huber-Reggi, S. P., Salierno, F. G., Manfredi, A., Neuhauss, S. C. F., Banfi, S. and Conte, I. (2015b). miR-181a/b control the assembly of visual circuitry by regulating retinal axon specification and growth. *Dev. Neurobiol.* **75**, 1252-1267. doi:10.1002/dneu.22282

Cepko, C. (2014). Intrinsically different retinal progenitor cells produce specific types of progeny. *Nat. Rev. Neurosci.* **15**, 615-627. doi:10.1038/nrn3767

Chan, C. S. Y., Lonfat, N., Zhao, R., Davis, A. E., Li, L., Wu, M.-R., Lin, C.-H., Ji, Z., Cepko, C. L. and Wang, S. (2020). Cell type- and stage-specific expression of Otx2 is regulated by multiple transcription factors and cis-regulatory modules in the retina. *Development* **147**, dev187922. doi:10.1242/dev.187922

Chi, S. W., Zang, J. B., Mele, A. and Darnell, R. B. (2009). Argonaute HITS-CLIP decodes microRNA-mRNA interaction maps. *Nature* **460**, 479-486. doi:10.1038/nature08170

Choi, H. M. T., Schwarzkopf, M., Fornace, M. E., Acharya, A., Artavanis, G., Stegmaier, J., Cunha, A. and Pierce, N. A. (2018). Third-generation in situ hybridization chain reaction: multiplexed, quantitative, sensitive, versatile, robust. *Development* **145**, dev165753. doi:10.1242/dev.165753

Chung, K.-H., Hart, C. C., Al-Bassam, S., Avery, A., Taylor, J., Patel, P. D., Vojtek, A. B. and Turner, D. L. (2006). Polycistronic RNA polymerase II expression vectors for RNA interference based on BIC/miR-155. *Nucleic Acids Res.* **34**, e53. doi:10.1093/nar/gkl143

Clark, B. S., Stein-O'Brien, G. L., Shiau, F., Cannon, G. H., Davis-Marcisak, E., Sherman, T., Santiago, C. P., Hoang, T. V., Rajaii, F., James-Esposito, R. E. et al. (2019). Single-cell RNA-seq analysis of retinal development identifies NFI factors as regulating mitotic exit and late-born cell specification. *Neuron* **102**, 1111-1126.e1115. doi:10.1016/j.neuron.2019.04.010

Clement, K., Rees, H., Canver, M. C., Gehrke, J. M., Farouni, R., Hsu, J. Y., Cole, M. A., Liu, D. R., Joung, J. K., Bauer, D. E. et al. (2019). CRISPResso2 provides accurate and rapid genome editing sequence analysis. *Nat. Biotechnol.* **37**, 224-226. doi:10.1038/s41587-019-0032-3

Damiani, D., Alexander, J. J., O'Rourke, J. R., McManus, M., Jadhav, A. P., Cepko, C. L., Hauswirth, W. W., Harfe, B. D. and Strettoi, E. (2008). Dicer inactivation leads to progressive functional and structural degeneration of the mouse retina. *J. Neurosci.* **28**, 4878-4887. doi:10.1523/JNEUROSCI.0828-08.2008

Dang, Y., Jia, G., Choi, J., Ma, H., Anaya, E., Ye, C., Shankar, P. and Wu, H. (2015). Optimizing sgRNA structure to improve CRISPR-Cas9 knockout efficiency. *Genome Biol.* **16**, 823. doi:10.1186/s13059-015-0846-3

Davis, N., Mor, E. and Ashery-Padan, R. (2011). Roles for Dicer1 in the patterning and differentiation of the optic cup neuroepithelium. *Development* **138**, 127-138. doi:10.1242/dev.053637

Del Barrio, M. G., Taveira-Marques, R., Muroyama, Y., Yuk, D.-I., Li, S., Wines-Samuelson, M., Shen, J., Smith, H. K., Xiang, M., Rowitch, D. et al. (2007). A regulatory network involving Foxn4, Mash1 and delta-like 4/Notch1 generates V2a and V2b spinal interneurons from a common progenitor pool. *Development* **134**, 3427-3436. doi:10.1242/dev.005868

Deo, M., Yu, J.-Y., Chung, K.-H., Tippens, M. and Turner, D. L. (2006). Detection of mammalian microRNA expression by in situ hybridization with RNA oligonucleotides. *Dev. Dyn.* **235**, 2538-2548. doi:10.1002/dvdy.20847

Dobin, A. and Gingeras, T. R. (2016). Optimizing RNA-seq mapping with STAR. *Methods Mol. Biol.* **1415**, 245-262. doi:10.1007/978-1-4939-3572-7_13

Edmonson, M. N., Zhang, J., Yan, C., Finney, R. P., Meerzaman, D. M. and Buetow, K. H. (2011). Bambino: a variant detector and alignment viewer for next-generation sequencing data in the SAM/BAM format. *Bioinformatics* **27**, 865-866. doi:10.1093/bioinformatics/btr032

Farah, M. H., Olson, J. M., Sucic, H. B., Hume, R. I., Tapscott, S. J. and Turner, D. L. (2000). Generation of neurons by transient expression of neural bHLH proteins in mammalian cells. *Development* **127**, 693-702. doi:10.1242/dev.127.4.693

Frankish, A., Diekhans, M., Ferreira, A.-M., Johnson, R., Jungreis, I., Loveland, J., Mudge, J. M., Sisu, C., Wright, J., Armstrong, J. et al. (2019). GENCODE reference annotation for the human and mouse genomes. *Nucleic Acids Res.* **47**, D766-D773. doi:10.1093/nar/gky955

Fujitani, Y., Fujitani, S., Luo, H., Qiu, F., Burlison, J., Long, Q., Kawaguchi, Y., Edlund, H., Macdonald, R. J., Furukawa, T. et al. (2006). Ptf1a determines horizontal and amacrine cell fates during mouse retinal development. *Development* **133**, 4439-4450. doi:10.1242/dev.02598

Georgi, S. A. and Reh, T. A. (2010). Dicer is required for the transition from early to late progenitor state in the developing mouse retina. *J. Neurosci.* **30**, 4048-4061. doi:10.1523/JNEUROSCI.4982-09.2010

Goodson, N. B., Kaufman, M. A., Park, K. U. and Brzezinski, J. A.IV. (2020). Simultaneous deletion of Prdm1 and Vsx2 enhancers in the retina alters photoreceptor and bipolar cell fate specification, yet differs from deleting both genes. *Development* **147**, dev190272. doi:10.1242/dev.190272

Gupta, S., M-Redmond, T., Meng, F., Tidball, A., Akil, H., Watson, S., Parent, J. M. and Uhler, M. (2018). Fibroblast growth factor 2 regulates activity and gene expression of human post-mitotic excitatory neurons. *J. Neurochem.* **145**, 188-203. doi:10.1111/jnc.14255

Hafner, M., Landthaler, M., Burger, L., Khorshid, M., Hausser, J., Berninger, P., Rothballer, A., Ascano, M., Jr, Jungkamp, A.-C., Munschauer, M. et al. (2010). Transcriptome-wide identification of RNA-binding protein and microRNA target sites by PAR-CLIP. *Cell* **141**, 129-141. doi:10.1016/j.cell.2010.03.009

Han, T.-S., Voon, D. C.-C., Oshima, H., Nakayama, M., Echizen, K., Sakai, E., Yong, Z. W. E., Murakami, K., Yu, L., Minamoto, T. et al. (2019). Interleukin 1 up-regulates microRNA 135b to promote inflammation-associated gastric carcinogenesis in mice. *Gastroenterology* **156**, 1140-1155.e1144. doi:10.1053/j.gastro.2018.11.059

Heigwer, F., Kerr, G. and Boutros, M. (2014). E-CRISP: fast CRISPR target site identification. *Nat. Methods* **11**, 122-123. doi:10.1038/nmeth.2812

Huang, X.-F., Huang, Z.-Q., Fang, X.-L., Chen, Z.-J., Cheng, W. and Jin, Z.-B. (2018). Retinal miRNAs variations in a large cohort of inherited retinal disease. *Ophthalmic Genet.* **39**, 175-179. doi:10.1080/13816810.2017.1329448

Huot, G., Vernier, M., Bourdeau, V., Doucet, L., Saint-Germain, E., Gaumont-Leclerc, M.-F., Moro, A. and Ferbeyre, G. (2014). CHES1/FOXN3 regulates cell proliferation by repressing PIM2 and protein biosynthesis. *Mol. Biol. Cell* **25**, 554-565. doi:10.1091/mbc.e13-02-0110

Inoue, T., Hojo, M., Bessho, Y., Tano, Y., Lee, J. E. and Kageyama, R. (2002). Math3 and NeuroD regulate amacrine cell fate specification in the retina. *Development* **129**, 831-842. doi:10.1242/dev.129.4.831

Islam, M. M., Li, Y., Luo, H., Xiang, M. and Cai, L. (2013). Meis1 regulates Foxn4 expression during retinal progenitor cell differentiation. *Biology open* **2**, 1125-1136. doi:10.1242/bio.20132279

Kara, N., Kent, M. R., Didiano, D., Rajaram, K., Zhao, A., Summerbell, E. R. and Patton, J. G. (2019). The miR-216a-Dot1l regulatory axis is necessary and sufficient for Müller Glia reprogramming during retina regeneration. *Cell Rep.* **28**, 2037-2047.e34. doi:10.1016/j.celrep.2019.07.061

Karanth, S., Adams, J. D., Serrano, M. d. l. A., Quittner-Strom, E. B., Simcox, J., Villanueva, C. J., Ozcan, L., Holland, W. L., Yost, H. J., Vella, A. et al. (2018). A hepatocyte FOXN3-α cell glucagon axis regulates fasting glucose. *Cell Rep.* **24**, 312-319. doi:10.1016/j.celrep.2018.06.039

Kato, M., Putta, S., Wang, M., Yuan, H., Lanting, L., Nair, I., Gunn, A., Nakagawa, Y., Shimano, H., Todorov, I. et al. (2009). TGF-beta activates Akt kinase through a microRNA-dependent amplifying circuit targeting PTEN. *Nat. Cell Biol.* **11**, 881-889. doi:10.1038/ncb1897

Kawaguchi, Y., Cooper, B., Gannon, M., Ray, M., MacDonald, R. J. and Wright, C. V. E. (2002). The role of the transcriptional regulator Ptf1a in converting intestinal to pancreatic progenitors. *Nat. Genet.* **32**, 128-134. doi:10.1038/ng959

Konstantinides, N., Rossi, A. M. and Desplan, C. (2015). Common temporal identity factors regulate neuronal diversity in fly ventral nerve cord and mouse retina. *Neuron* **85**, 447-449. doi:10.1016/j.neuron.2015.01.016

Kozomara, A., Birgaoanu, M. and Griffiths-Jones, S. (2019). miRBase: from microRNA sequences to function. *Nucleic Acids Res.* **47**, D155-D162. doi:10.1093/nar/gky1141

Lelièvre, E. C., Benayoun, B. A., Mahieu, L., Roger, J. E., Sahel, J.-A., Sennlaub, F., Veitia, R. A., Goureau, O. and Guillonneau, X. (2012). A regulatory domain is required for Foxn4 activity during retinogenesis. *J. Mol. Neurosci.* **46**, 315-323. doi:10.1007/s12031-011-9585-4

Li, H. and Edlund, H. (2001). Persistent expression of Hlxb9 in the pancreatic epithelium impairs pancreatic development. *Dev. Biol.* **240**, 247-253. doi:10.1006/dbio.2001.0440

Li, S., Mo, Z., Yang, X., Price, S. M., Shen, M. M. and Xiang, M. (2004). Foxn4 controls the genesis of amacrine and horizontal cells by retinal progenitors. *Neuron* **43**, 795-807. doi:10.1016/j.neuron.2004.08.041

Li, W., Zhang, Z., Liu, X., Cheng, X., Zhang, Y., Han, X., Zhang, Y., Liu, S., Yang, J., Xu, B. et al. (2017). The FOXN3-NEAT1-SIN3A repressor complex promotes progression of hormonally responsive breast cancer. *J. Clin. Investig.* **127**, 3421-3440. doi:10.1172/JCI94233

Lipchina, I., Elkabetz, Y., Hafner, M., Sheridan, R., Mihailovic, A., Tuschl, T., Sander, C., Studer, L. and Betel, D. (2011). Genome-wide identification of microRNA targets in human ES cells reveals a role for miR-302 in modulating BMP response. *Genes Dev.* **25**, 2173-2186. doi:10.1101/gad.17221311

Liu, H., Kim, S.-Y., Fu, Y., Wu, X., Ng, L., Swaroop, A. and Forrest, D. (2013). An isoform of retinoid-related orphan receptor β directs differentiation of retinal amacrine and horizontal interneurons. *Nat. Commun.* **4**, 1813. doi:10.1038/ncomms2793

Liu, S., Liu, X., Li, S., Huang, X., Qian, H., Jin, K. and Xiang, M. (2020). Foxn4 is a temporal identity factor conferring mid/late-early retinal competence and involved in retinal synaptogenesis. *Proc. Natl Acad. Sci. USA* **117**, 5016-5027. doi:10.1073/pnas.1918628117

Luo, H., Jin, K., Xie, Z., Qiu, F., Li, S., Zou, M., Cai, L., Hozumi, K., Shima, D. T. and Xiang, M. (2012). Forkhead box N4 (Foxn4) activates Dll4-Notch signaling to suppress photoreceptor cell fates of early retinal progenitors. *Proc. Natl. Acad. Sci. USA* **109**, E553-E562. doi:10.1073/pnas.1115767109

Ma, L., Cantrup, R., Varrault, A., Colak, D., Klenin, N., Götz, M., McFarlane, S., Journot, L. and Schuurmans, C. (2007). Zac1 functions through TGFβII to negatively regulate cell number in the developing retina. *Neural Dev.* **2**, 11. doi:10.1186/1749-8104-2-11

Ma, J., Lu, Y., Zhang, S., Li, Y., Huang, J., Yin, Z., Ren, J., Huang, K., Liu, L., Yang, K. et al. (2018). β-Trcp ubiquitin ligase and RSK2 kinase-mediated degradation of FOXN2 promotes tumorigenesis and radioresistance in lung cancer. *Cell Death Differ.* **25**, 1473-1485. doi:10.1038/s41418-017-0055-6

MacNeil, M. A. and Masland, R. H. (1998). Extreme diversity among amacrine cells: implications for function. *Neuron* **20**, 971-982. doi:10.1016/S0896-6273(00)80478-X

Macosko, E. Z., Basu, A., Satija, R., Nemesh, J., Shekhar, K., Goldman, M., Tirosh, I., Bialas, A. R., Kamitaki, N., Martersteck, E. M. et al. (2015). Highly parallel genome-wide expression profiling of individual cells using nanoliter droplets. *Cell* **161**, 1202-1214. doi:10.1016/j.cell.2015.05.002

Masland, R. H. (2012). The tasks of amacrine cells. *Vis. Neurosci.* **29**, 3-9. doi:10.1017/S0952523811000344

Matsuda, T. and Cepko, C. L. (2004). Electroporation and RNA interference in the rodent retina in vivo and in vitro. *Proc. Natl. Acad. Sci. USA* **101**, 16-22. doi:10.1073/pnas.2235688100

Mattar, P., Ericson, J., Blackshaw, S. and Cayouette, M. (2015). A conserved regulatory logic controls temporal identity in mouse neural progenitors. *Neuron* **85**, 497-504. doi:10.1016/j.neuron.2014.12.052

Nakagawa, S., Gisselbrecht, S. S., Rogers, J. M., Hartl, D. L. and Bulyk, M. L. (2013). DNA-binding specificity changes in the evolution of forkhead transcription factors. *Proc. Natl. Acad. Sci. USA* **110**, 12349-12354. doi:10.1073/pnas.1310430110

Nakhai, H., Sel, S., Favor, J., Mendoza-Torres, L., Paulsen, F., Duncker, G. I. W. and Schmid, R. M. (2007). Ptf1a is essential for the differentiation of GABAergic and glycinergic amacrine cells and horizontal cells in the mouse retina. *Development* **134**, 1151-1160. doi:10.1242/dev.02781

Nelson, P. T., De Planell-Saguer, M., Lamprinaki, S., Kiriakidou, M., Zhang, P., O'Doherty, U. and Mourelatos, Z. (2007). A novel monoclonal antibody against human Argonaute proteins reveals unexpected characteristics of miRNAs in human blood cells. *RNA (New York, NY)* **13**, 1787-1792. doi:10.1261/rna.646007

Olena, A. F., Rao, M. B., Thatcher, E. J., Wu, S.-Y. and Patton, J. G. (2015). miR-216a regulates snx5, a novel notch signaling pathway component, during zebrafish retinal development. *Dev. Biol.* **400**, 72-81. doi:10.1016/j.ydbio.2015.01.016

Quinlan, A. R. (2014). BEDTools: The Swiss-army tool for genome feature analysis. *Curr. Protoc. Bioinformatics* **47**, 11.12.1-11.12.34. doi:10.1002/0471250953.bi1112s47

Ran, F. A., Hsu, P. D., Wright, J., Agarwala, V., Scott, D. A. and Zhang, F. (2013). Genome engineering using the CRISPR-Cas9 system. *Nat. Protoc.* **8**, 2281-2308. doi:10.1038/nprot.2013.143

Ravishankar, H., Mangani, A. S., Phoebe Moses, G. L., Mani, S. P., Parameswaran, S., Khetan, V., Ganesan, S. and Krishnakumar, S. (2020). Serum exosomal miRNA as biomarkers for Retinoblastoma. *Exp. Eye Res.* **199**, 108184. doi:10.1016/j.exer.2020.108184

Reh, T. A. and Hindges, R. (2018). MicroRNAs in retinal development. *Annu. Rev. Vis. Sci.* **4**, 25-44. doi:10.1146/annurev-vision-091517-034357

Rogers, J. M., Waters, C. T., Seegar, T. C. M., Jarrett, S. M., Hallworth, A. N., Blacklow, S. C. and Bulyk, M. L. (2019). Bispecific Forkhead transcription factor FoxN3 recognizes two distinct motifs with different DNA shapes. *Mol. Cell* **74**, 245-253.e246. doi:10.1016/j.molcel.2019.01.019

Samaan, G., Yugo, D., Rajagopalan, S., Wall, J., Donnell, R., Goldowitz, D., Gopalakrishnan, R. and Venkatachalam, S. (2010). Foxn3 is essential for craniofacial development in mice and a putative candidate involved in human congenital craniofacial defects. *Biochem. Biophys. Res. Commun.* **400**, 60-65. doi:10.1016/j.bbrc.2010.07.142

Sarin, S., Zuniga-Sanchez, E., Kurmangaliyev, Y. Z., Cousins, H., Patel, M., Hernandez, J., Zhang, K. X., Samuel, M. A., Morey, M., Sanes, J. R. et al. (2018). Role for Wnt signaling in retinal neuropil development: analysis via RNA-seq and in vivo somatic CRISPR mutagenesis. *Neuron* **98**, 109-126.e8. doi:10.1016/j.neuron.2018.03.004

Sarshad, A. A., Juan, A. H., Muler, A. I. C., Anastasakis, D. G., Wang, X., Genzor, P., Feng, X., Tsai, P.-F., Sun, H.-W., Haase, A. D. et al. (2018). Argonaute-miRNA complexes silence target mRNAs in the nucleus of mammalian stem cells. *Mol. Cell* **71**, 1040-1050.e48. doi:10.1016/j.molcel.2018.07.020

Schuff, M., Rössner, A., Wacker, S. A., Donow, C., Gessert, S. and Knöchel, W. (2007). FoxN3 is required for craniofacial and eye development of Xenopus laevis. *Dev. Dyn.* **236**, 226-239. doi:10.1002/dvdy.21007

Scott, K. L. and Plon, S. E. (2005). CHES1/FOXN3 interacts with Ski-interacting protein and acts as a transcriptional repressor. *Gene* **359**, 119-126. doi:10.1016/j.gene.2005.06.014

Shekhar, K., Lapan, S. W., Whitney, I. E., Tran, N. M., Macosko, E. Z., Kowalczyk, M., Adiconis, X., Levin, J. Z., Nemesh, J., Goldman, M. et al. (2016). Comprehensive classification of retinal bipolar neurons by single-cell transcriptomics. *Cell* **166**, 1308-1323.e30. doi:10.1016/j.cell.2016.07.054

Siepel, A., Bejerano, G., Pedersen, J. S., Hinrichs, A. S., Hou, M., Rosenbloom, K., Clawson, H., Spieth, J., Hillier, L. W. D., Richards, S. et al. (2005). Evolutionarily conserved elements in vertebrate, insect, worm, and yeast genomes. *Genome Res.* **15**, 1034-1050. doi:10.1101/gr.3715005

Sutaria, D. S., Jiang, J., Azevedo-Pouly, A. C., Wright, L., Bray, J. A., Fredenburg, K., Liu, X., Lu, J., Torres, C., Mancinelli, G. et al. (2019). Knockout of acinar enriched microRNAs in mice promote duct formation but not pancreatic cancer. *Sci. Rep.* **9**, 11147. doi:10.1038/s41598-019-47566-x

Tachibana, N., Cantrup, R., Dixit, R., Touahri, Y., Kaushik, G., Zinyk, D., Daftarian, N., Biernaskie, J., McFarlane, S. and Schuurmans, C. (2016). Pten regulates retinal amacrine cell number by modulating Akt, Tgfβ, and Erk signaling. *J. Neurosci.* **36**, 9454-9471. doi:10.1523/JNEUROSCI.0936-16.2016

Thomson, J. M., Newman, M., Parker, J. S., Morin-Kensicki, E. M., Wright, T. and Hammond, S. M. (2006). Extensive post-transcriptional regulation of microRNAs and its implications for cancer. *Genes Dev.* **20**, 2202-2207.

Thorvaldsdottir, H., Robinson, J. T. and Mesirov, J. P. (2013). Integrative Genomics Viewer (IGV): high-performance genomics data visualization and exploration. *Brief. Bioinform.* **14**, 178-192. doi:10.1093/bib/bbs017

Turner, D. L., Snyder, E. Y. and Cepko, C. L. (1990). Lineage-independent determination of cell type in the embryonic mouse retina. *Neuron* **4**, 833-845. doi:10.1016/0896-6273(90)90136-4

Voinescu, P. E., Kay, J. N. and Sanes, J. R. (2009). Birthdays of retinal amacrine cell subtypes are systematically related to their molecular identity and soma position. *J. Comp. Neurol.* **517**, 737-750. doi:10.1002/cne.22200

Walker, J. C. and Harland, R. M. (2009). microRNA-24a is required to repress apoptosis in the developing neural retina. *Genes Dev.* **23**, 1046-1051. doi:10.1101/gad.1777709

Wang, S., Sengel, C., Emerson, M. M. and Cepko, C. L. (2014). A gene regulatory network controls the binary fate decision of rod and bipolar cells in the vertebrate retina. *Dev. Cell* **30**, 513-527. doi:10.1016/j.devcel.2014.07.018

Wienholds, E., Kloosterman, W. P., Miska, E., Alvarez-Saavedra, E., Berezikov, E., de Bruijn, E., Horvitz, H. R., Kauppinen, S. and Plasterk, R. H. A. (2005). MicroRNA expression in zebrafish embryonic development. *Science* **309**, 310-311. doi:10.1126/science.1114519

Wohl, S. G., Jorstad, N. L., Levine, E. M. and Reh, T. A. (2017). Müller glial microRNAs are required for the maintenance of glial homeostasis and retinal architecture. *Nat. Commun.* **8**, 1603. doi:10.1038/s41467-017-01624-y

Wohl, S. G., Hooper, M. J. and Reh, T. A. (2019). MicroRNAs miR-25, let-7 and miR-124 regulate the neurogenic potential of Müller glia in mice. *Development* **146**, dev179556. doi:10.1242/dev.179556

Xiang, L., Chen, X.-J., Wu, K.-C., Zhang, C.-J., Zhou, G.-H., Lv, J.-N., Sun, L.-F., Cheng, F.-F., Cai, X.-B. and Jin, Z.-B. (2017). miR-183/96 plays a pivotal regulatory role in mouse photoreceptor maturation and maintenance. *Proc. Natl. Acad. Sci. USA* **114**, 6376-6381. doi:10.1073/pnas.1618757114

Xu, S., Witmer, P. D., Lumayag, S., Kovacs, B. and Valle, D. (2007). MicroRNA (miRNA) transcriptome of mouse retina and identification of a sensory organ-specific miRNA cluster. *J. Biol. Chem.* **282**, 25053-25066. doi:10.1074/jbc.M700501200

Yan, W., Laboulaye, M. A., Tran, N. M., Whitney, I. E., Benhar, I. and Sanes, J. R. (2020). Mouse retinal cell atlas: molecular identification of over sixty Amacrine cell types. *J. Neurosci.* **40**, 5177-5195. doi:10.1523/JNEUROSCI.0471-20.2020

Zeng, C., Pan, F., Jones, L. A., Lim, M. M., Griffin, E. A., Sheline, Y. I., Mintun, M. A., Holtzman, D. M. and Mach, R. H. (2010). Evaluation of 5-ethynyl-2′-deoxyuridine staining as a sensitive and reliable method for studying cell proliferation in the adult nervous system. *Brain Res.* **1319**, 21-32. doi:10.1016/j.brainres.2009.12.092

Zhang, H., Deo, M., Thompson, R. C., Uhler, M. D. and Turner, D. L. (2012). Negative regulation of Yap during neuronal differentiation. *Dev. Biol.* **361**, 103-115. doi:10.1016/j.ydbio.2011.10.017

Zhang, J., Hu, Z., Wen, C., Liao, Q., He, B., Peng, J., Tang, X., Chen, Z. and Xie, Y. (2021). MicroRNA-182 promotes epithelial-mesenchymal transition by targeting FOXN3 in gallbladder cancer. *Oncol. Lett.* **21**, 200. doi:10.3892/ol.2021.12461

Zhuang, P., Zhang, H., Welchko, R. M., Thompson, R. C., Xu, S. and Turner, D. L. (2020). Combined microRNA and mRNA detection in mammalian retinas by in situ hybridization chain reaction. *Sci. Rep.* **10**, 351. doi:10.1038/s41598-019-57194-0

Zou, M., Luo, H. and Xiang, M. (2015). Selective neuronal lineages derived from Dll4-expressing progenitors/precursors in the retina and spinal cord. *Dev. Dyn.* **244**, 86-97. doi:10.1002/dvdy.24185

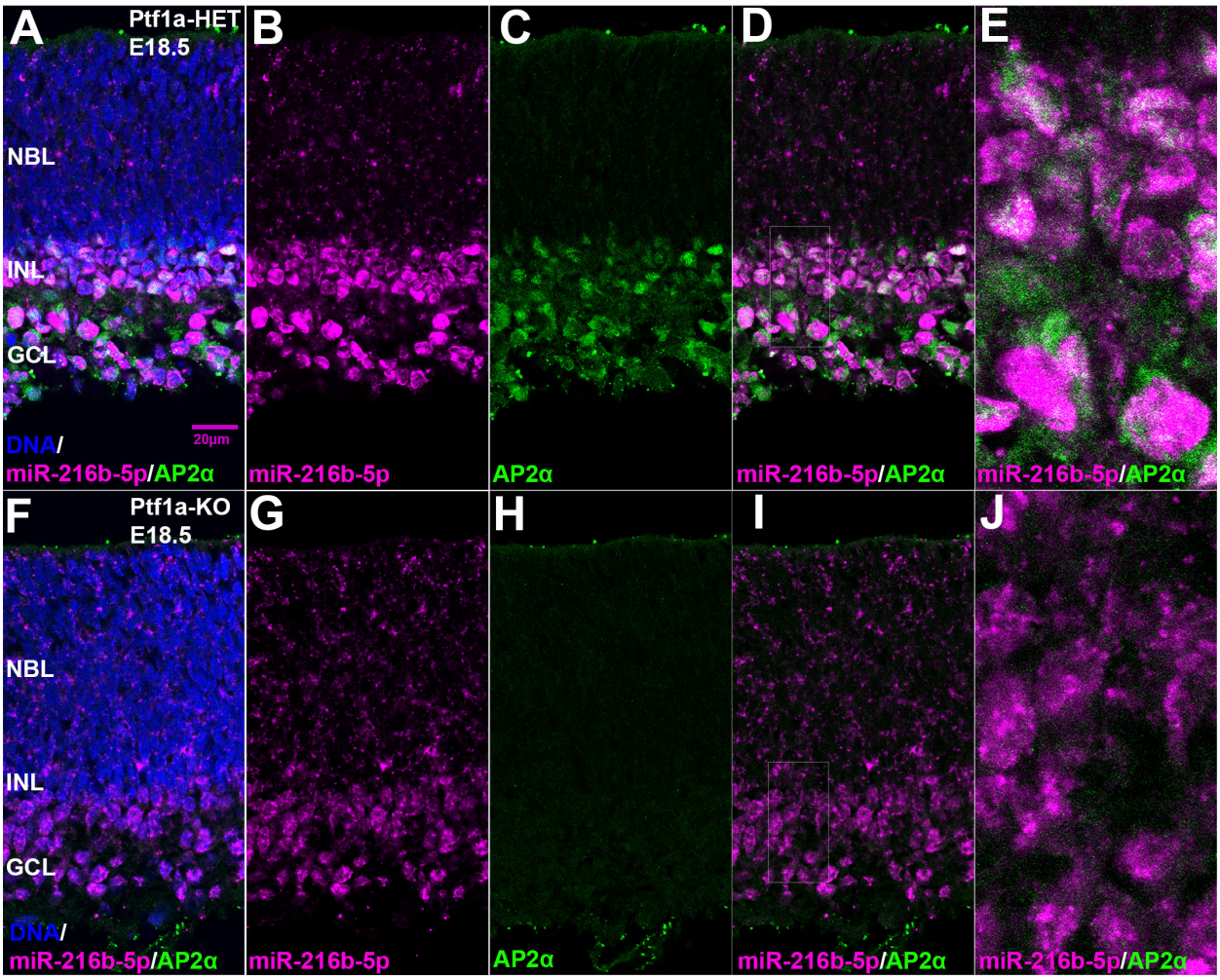

Fig. S1. **miR-216b expression in amacrine cells in E18.5 retinas.** (A-E) Mature miR-216b detected by fluorescent in situ hybridization (magenta) overlaps with AP2α (green) in retinas from mice heterozygous for Ptf1a.(F-J) Expression of mature miR-216b is reduced in the INL/GCL and AP2α is absent in retinas from mice homozygous for disruption of Ptf1a. (E) and (J) show enlargement of regions indicated in (D) or (I). Blue: nuclear DNA.

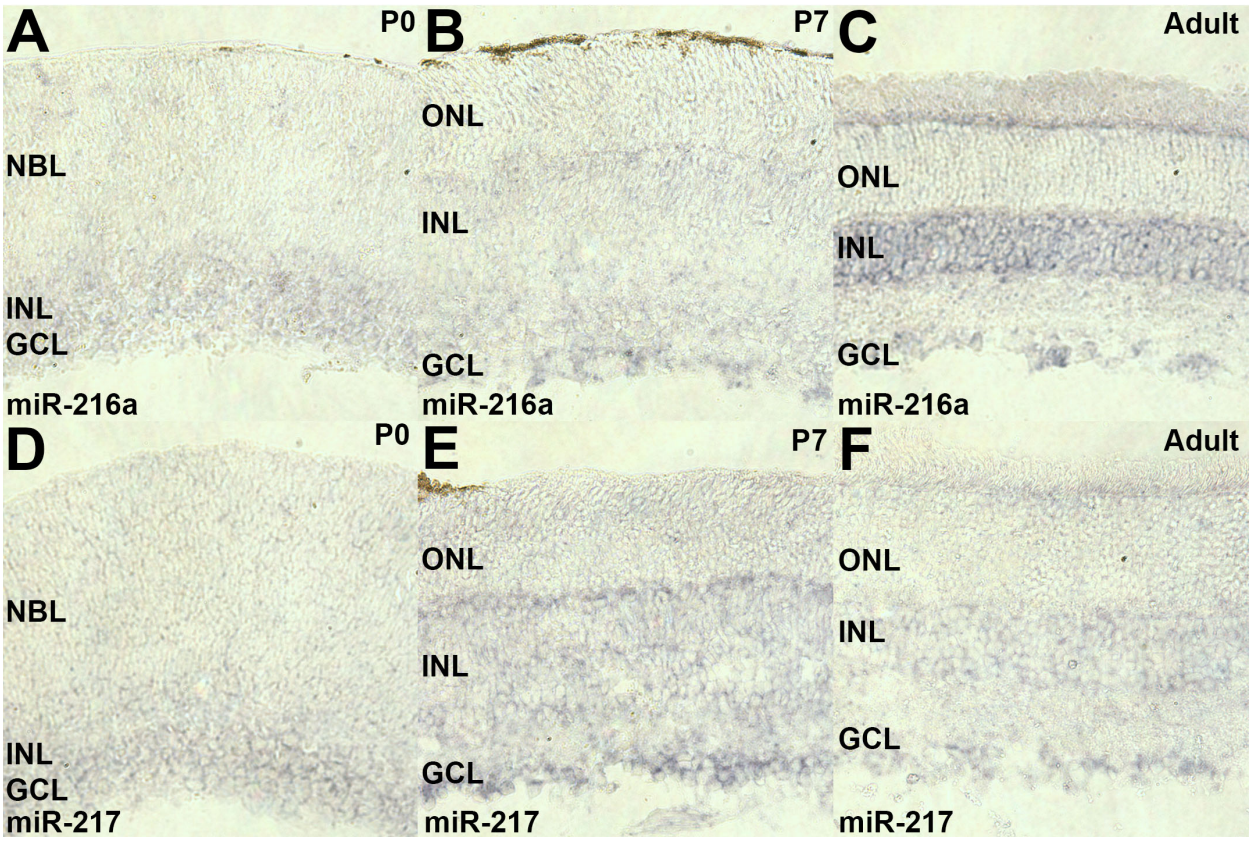

Fig.S2. **miR-216a and miR-217 expression in retina.** (A-C) Mature miR-216a detected by in situ hybridization (purple) is present in INL and GCL of P0, P7, and adult retinas. (D-F) Mature miR-217 is present in INL and GCL of P0, P7, and adult retinas.

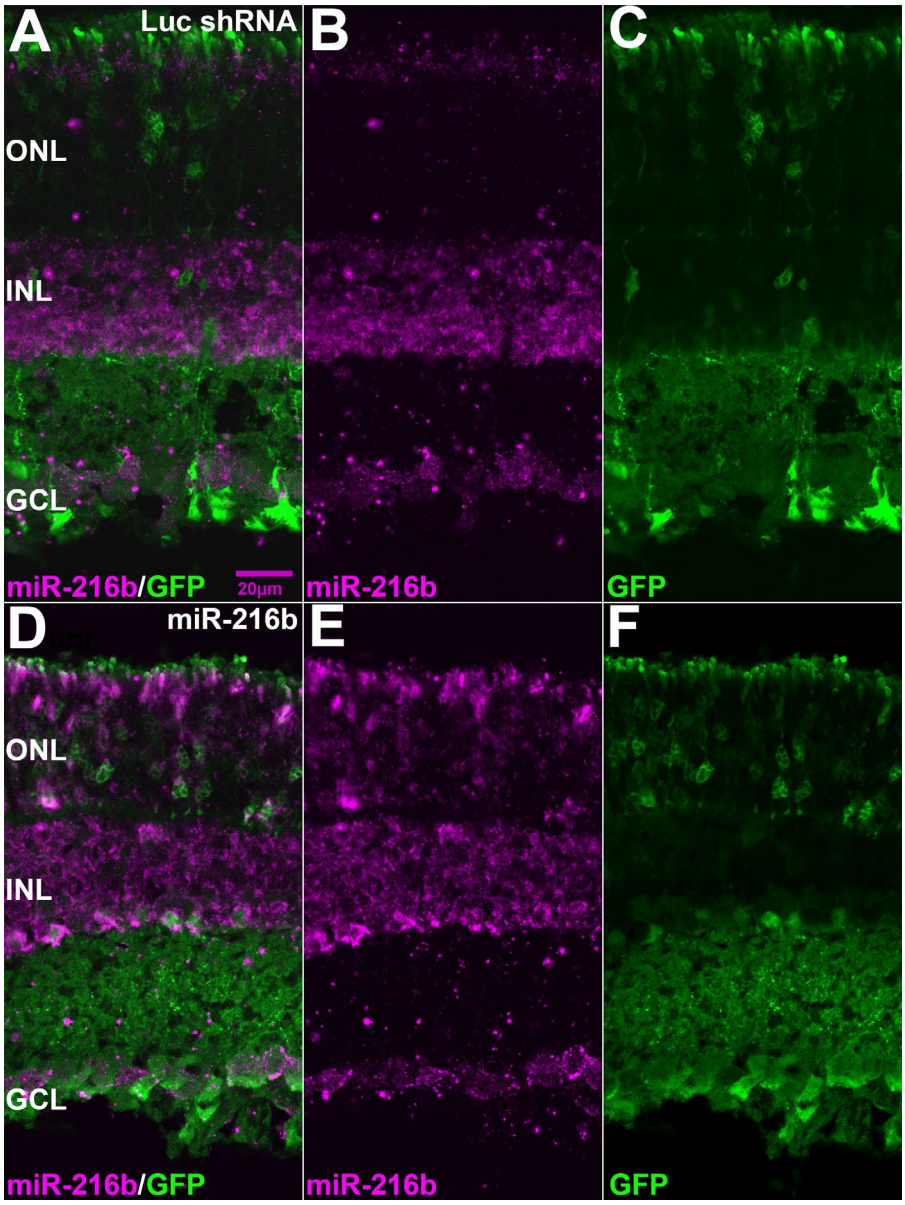

Fig. S3. **Detection of ectopic expression of the miR-216b miRNA in the mouse retina.** Plasmid vectors that co-express GFP with either miR-216b or a control Luc shRNA were introduced into the retina by *in vivo* electroporation at P0; retinas were fixed at P12 and processed in situ hybridization to detect mature miR-216- 5p (magenta) and indirect immunofluorescence to detect GFP (green). (A-C) In control retinas, widespread GFP-labeled cells are present in the ONL and INL, but high-level miR-216b-5p expression is restricted to the INL and GCL (sites of endogenous miR- 216b-5p expression) and low or absent in rods in the ONL. (D-F) In retinas electroporated with the miR-216b expression vector, ectopic miR-216b is detected in the rods of the ONL.

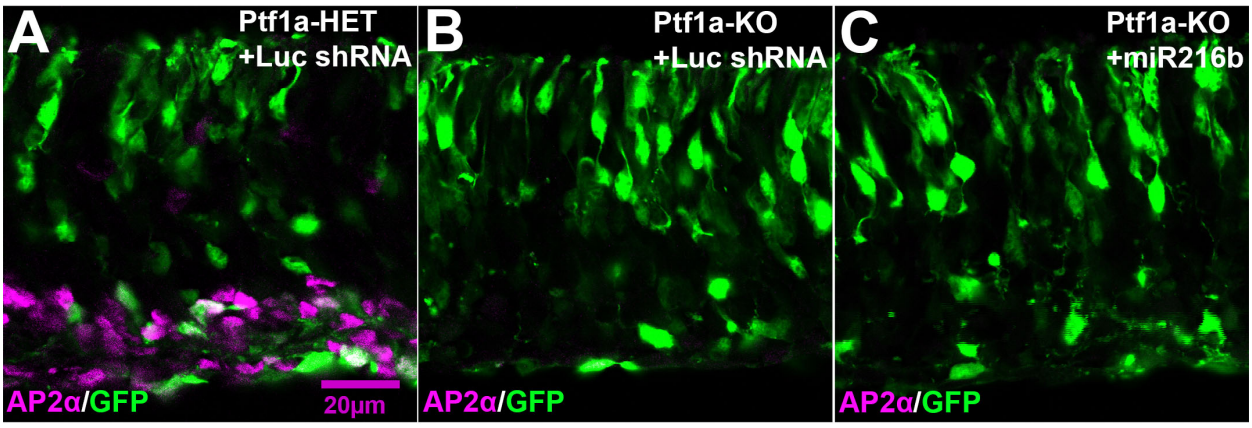

Fig. S4. **Ectopic expression of miR-216b in the developing retina does not generate amacrine cells in retinas from Ptf1a knockout mice.** Plasmid miRNA expression vectors which co-express GFP and either pre-miR-216b or the control Luc shRNA were introduced into retinas at E16.5 by electroporation, then the retinas were maintained in explant culture for 8DIV. (A) Control retina from a Ptf1a heterozygous mouse showing AP2α (magenta) overlaps with a subset of GFP-labeled cells (green). (B, C) In retina explants from mice homozygous for disruption of Ptf1a, AP2α labeled cells were not present among the GFP-labeled cells (representative images, N=3 for each vector in Ptf1a knockout retinas).

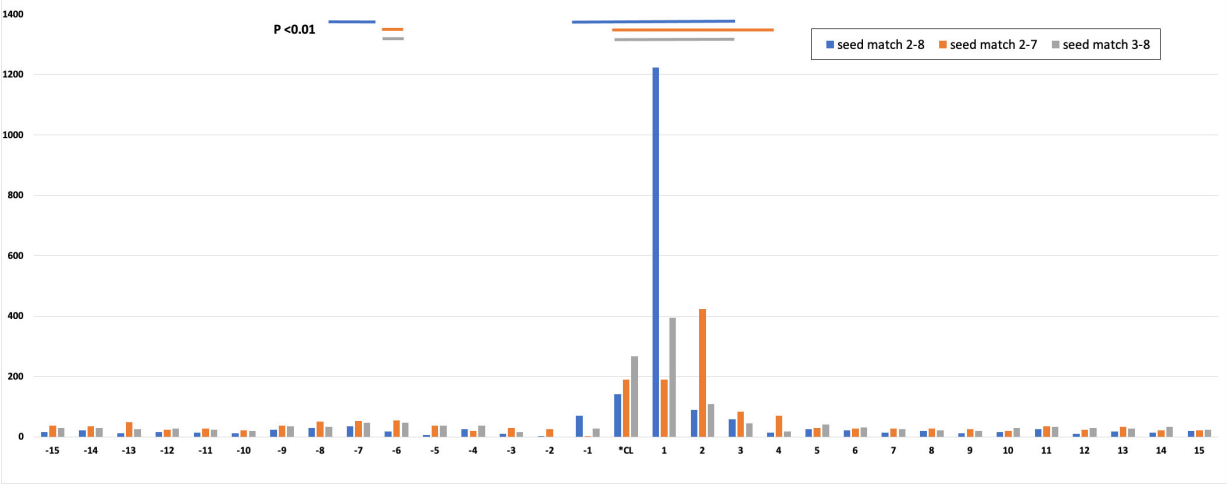

Fig. S5. miRNA seed matches are enriched near the predominant crosslinks in retina Argonaute PAR-CLIP libraries. We mapped common retinal miRNA seed sequences in 31 nt windows around 7237 predominant crosslink sites in 3' UTR exons. Crosslink sites near exon borders were excluded to avoid seed mappings outside of the exons. Seed matches were mapped at the 5' most base of each match, relative to each predominant crosslink site. The graph shows the count of 6 or 7 nt seed matches within +/-15 nt of a predominant crosslink site (*CL), summed across all sites. Only the longest match to a seed was counted (i.e. a 2-7 match or a 3-8 match located within a 2-8 match were not counted). Positions with enrichment ($P < 0.01$; Bonferonni correction used to adjust P values for multiple testing) for each type of seed match are indicated by matching color lines above the graph. Seed matches which overlap the crosslink site must have an A at the appropriate position in the seed to allow basepairing with the crosslinked U in the target, so fewer seeds can map at positions -6 to 0 (=*CL). DNA sequences for the 15 miRNA seeds used: miR-9-5p CTTTGGT, miR- 9-3p AAAGCTA, let-7ifagcdbe-5p/miR-98-5p GAGGTAG, miR-124-3p AAGGCAC, miR- 182-5p TTGGCAA, miR-183-5p ATGGCAC, miR-26ab-5p TCAAGTA, miR-181abdc-5p ACATTCA, miR-30dcaeb-5p GTAAACA, miR-148ab-3p/miR-152-3p CAGTGCA, miR-25-3p/miR-92ab-3p/miR-32-5p ATTGCAC, miR-99ba-5p/miR-100-5p ACCCGTA, miR-93-5p/miR-20a-5p/miR-17-5p/miR-106b-5p AAAGTGC, miR-125ab-5p/miR-351-5p CCCTGAG, miR-7ab-5p GGAAGAC. miRNAs with these seeds are expressed at P0 in the mouse retina (see Supplemental Table S2).

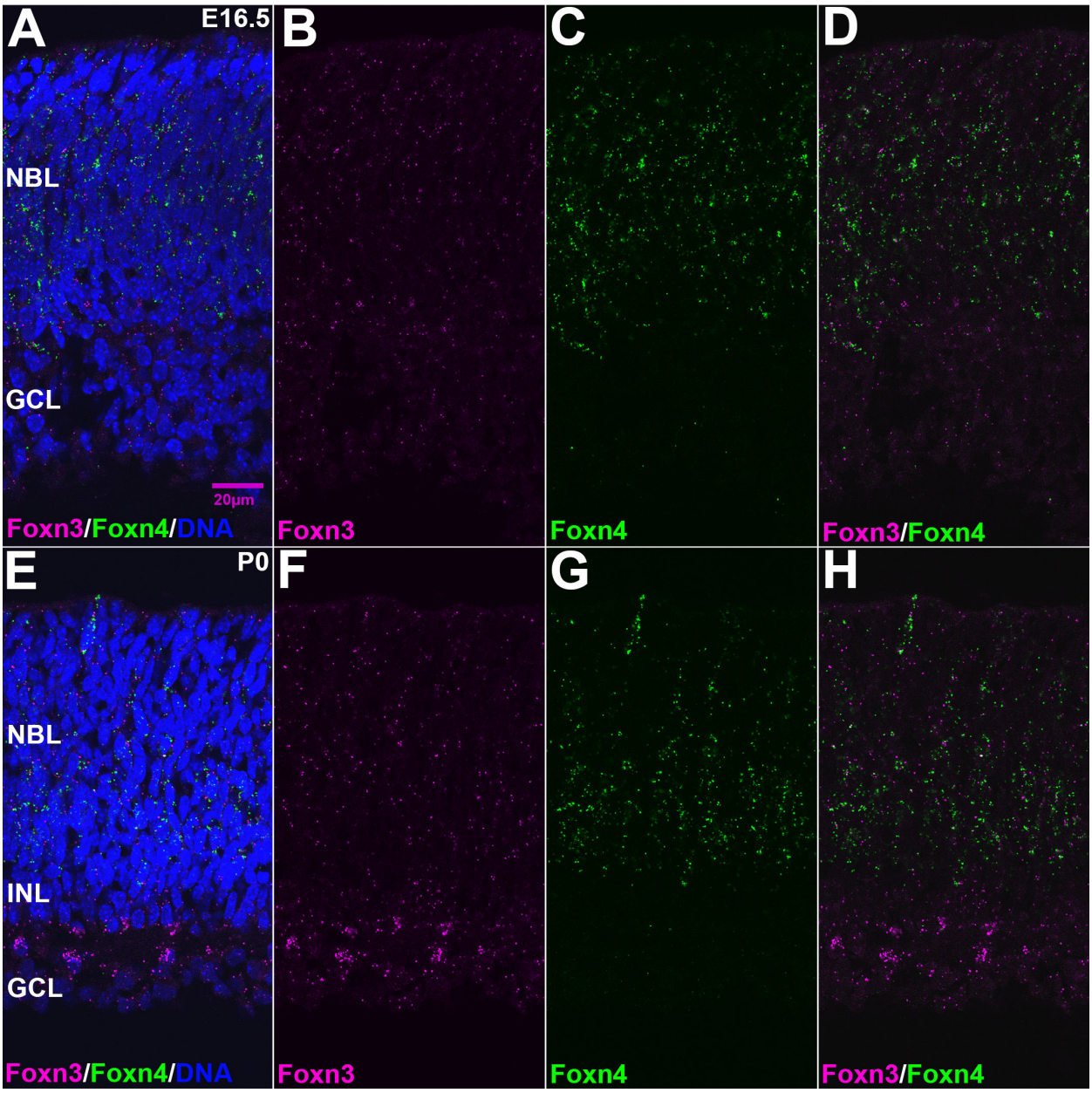

Fig. S6. Overlap between Foxn3 and Foxn4 expression in the developing retina.

(A-D) Foxn3 (magenta) and Foxn4 (green) expression in cells of the E16.5 retina, detected by in situ HCR. (E-H) Complete panels for Foxn3 and Foxn4 expression detected by in situ HCR in the P0 retina; Panel H is the same as Fig. 4G. Blue in A and E: nuclear DNA.

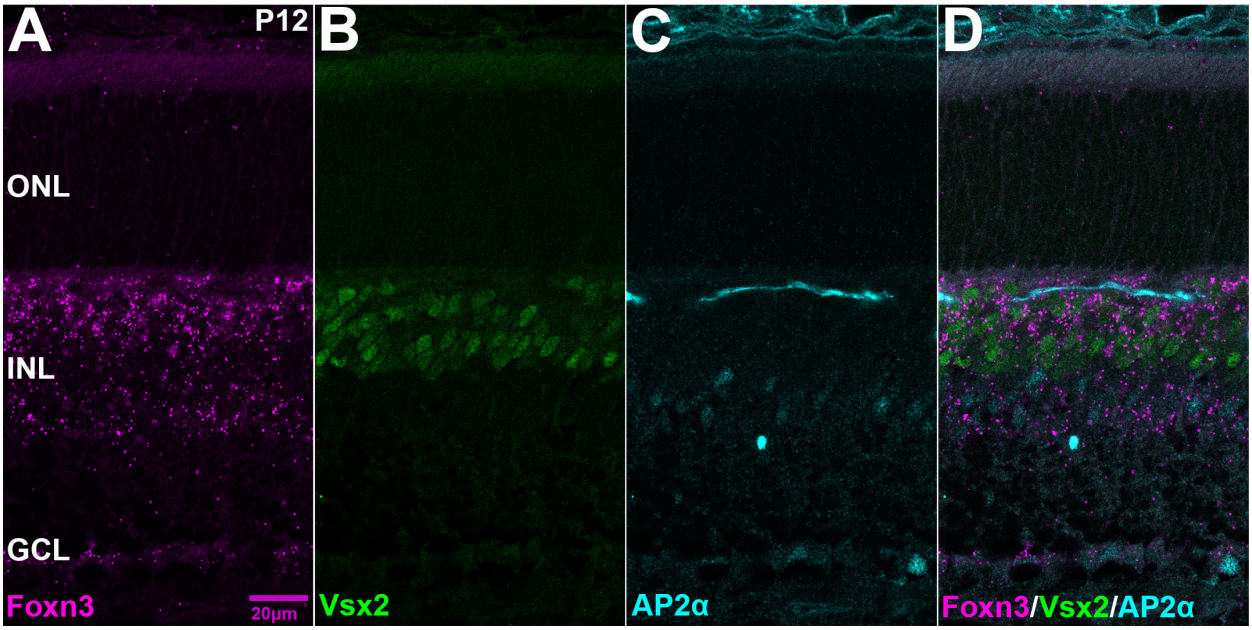

Fig. S7. Complete panels for Foxn3 and marker expression in the P12 retina. (A-D) Foxn3 mRNA in the INL at P12 (magenta), detected by in situ HCR, overlaps with Vsx2 (green) and AP2α (cyan) detected by immunofluorescence. Panel D is the same as Fig. 4L.

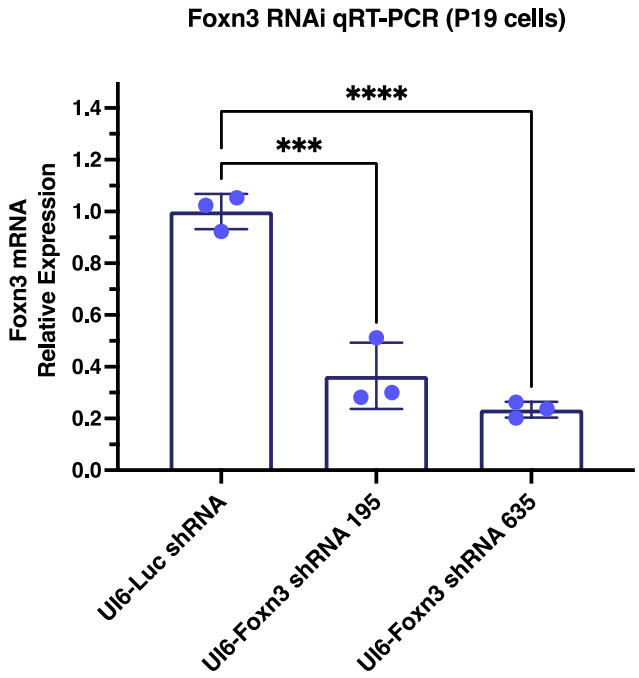

Fig. S8. Foxn3 RNAi reduces Foxn3 mRNA in a cell line. Mouse P19 cells were transfected with the control Luc-shRNA vector or one of two Foxn3 shRNA vectors. Foxn3 mRNA was measured by qRT-PCR. Both Foxn3 shRNAs reduced endogenous Foxn3 mRNA relative to the control (N=3). Significance based on one-way ANOVA with Dunnett's multiple comparisons test: *** $P < 0.001$, **** $P < 0.0001$. Graphs show mean ± s.d.

A

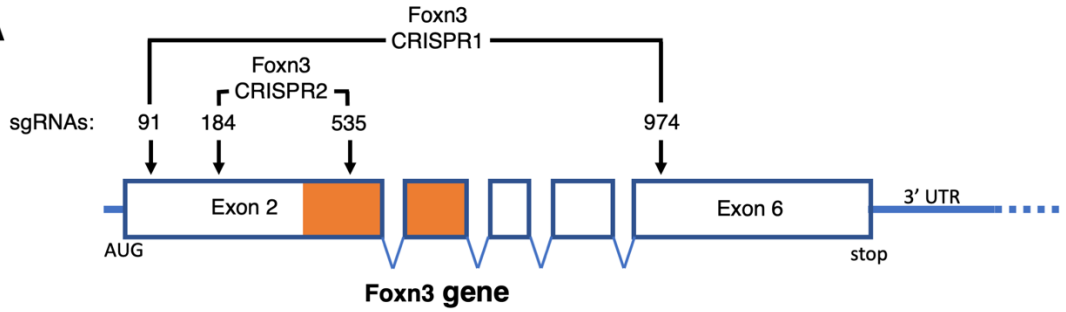

B

Foxn3 CRISPR1	Indel	Aligned Reads
sgRNA 91	0.69%	112,556
sgRNA 974	5.91%	47,513
control (91 target)	0.01%	48,440
control (974 target)	0.02%	44,292
Foxn3 CRISPR2		
sgRNA 184	0.01%	64,309
sgRNA 535	5.84%	57,015
control (184 target)	0.01%	69,888
control (535 target)	0.01%	58,123

Fig. S9. **CRISPR in retinal explants disrupts the Foxn3 gene.** (A) Schematic showing the location of sgRNA target sites within the coding exons of the Foxn3 gene on mouse Chr12. Orange indicates the Forkhead domain; introns are not to scale. Each CRISPR plasmid expresses two different sgRNAs as indicated. The 91 and 535 sgRNAs also match a Foxn3 pseudogene on mouse ChrX. The pseudogene does not appear to be expressed (no mRNA/EST sequences) and the coding potential of the pseudogene is disrupted by multiple frameshifts and mutations. (B) E16 retina explants were electroporated with a Foxn3 CRISPR vector or the parental CRISPR vector control. Genomic DNA was isolated two days later. Each of the four sgRNA target regions were PCR amplified and analyzed by Illumina sequencing. The number of reads and percentage of insertions/deletions (Indel) is listed for each sgRNA target site. For each of the two Foxn3 CRISPR vectors, one of the two sgRNAs was effective at generating indels. See Supplemental Table S6 for sequence alignments at each site.

Table S1. miRNA counts for small RNA seq of E16.5 retinas from mice heterozygous or homozygous for disruption of Ptf1a.

Click here to download Table S1

Table S2. miRNA counts for small RNA seq of P0 retinas from wild-type CD-1 mice.

Click here to download Table S2

Table S3. PAR-CLIP crosslink sites with a nearby sequence matching the seed sequences of both miR-216b and miR-216a.

Click here to download Table S3

Table S4. PAR-CLIP crosslink sites with a nearby sequence matching a seed sequence of either miR-216b or miR-216a but not both.

Click here to download Table S4

Table S5. Foxn3 mRNA expression in amacrine single cell RNA-seq data.

Click here to download Table S5

Table S6. Sequence analysis of Foxn3 CRISPR retina target sites.

Click here to download Table S6

Table S7. Sequences of oligonucleotide probes and primers.

Click here to download Table S7